When Irrigation Cannot Keep Pace: Aridification, Crop Composition, and the Spatial Concentration of Agricultural Water Use Efficiency Decline in Central Chile

(This paper is a non-peer reviewed preprint submitted to EarthArXiv)

Francisco Zambrano[a,*], Francisco Fernández[a], María Molinos-Senante[b]

[a] *Facultad de Economía, Negocios y Gobierno, Universidad San Sebastián, Santiago, Chile,*

[b] *Institute of Sustainable Processes, Universidad de Valladolid, Valladolid, Spain, 47011*

Abstract

Water scarcity under sustained aridification is among the most consequential threats to agriculture in Mediterranean-climate regions. Central Chile's ongoing megadrought (~2010-present), characterized by persistent precipitation deficits and intensified atmospheric evaporative demand-provides a natural experiment for examining how agricultural water use efficiency (WUE) responds to prolonged climatic stress. Using remotely sensed estimates of net primary production (NPP) and evapotranspiration (ET) across the 76 agricultural watersheds (2001-2020), we characterize WUE dynamics along multiple dimensions of aridification and assess the role of crop composition in modulating watershed-scale sensitivity.

Contrary to expectations that technological adaptation might buffer efficiency outcomes, we find a persistent, spatially coherent decline in agricultural WUE across much of central Chile, with structural break points clustering near 2010 in coincidence with megadrought onset. Hydroclimatic pressures-particularly reduced water availability and elevated atmospheric demand-appear to have outweighed any efficiency gains from improved irrigation practices, suggesting that under sustained drought, water and energy limitations constrain agricultural productivity at regional scales beyond the reach of field-level adaptation. Precipitation deficit was the dominant aridification signal explaining WUE variability, with atmospheric demand contributing modest independent explanatory power. Crop composition explained more than half of the spatial variance in drought sensitivity, with cereal-dominated systems showing lower WUE-SPEI sensitivity relative to forage systems, while irrigated area share was positively associated with drought sensitivity.

These results challenge the assumption that irrigation efficiency improvements can adequately buffer agriculture against intensifying hydroclimatic stress, and underscore the need for water governance frameworks

that operate at the landscape and regional scale.

Keywords: water use efficiency, megadrought, aridification, SPEI, Chile, NPP/ET, crop composition

1. Introduction

Global agriculture consumes approximately 70% of freshwater withdrawals (Hoekstra and Mekonnen, 2012), yet water use efficiency (WUE) remains poorly quantified at regional scales under conditions of sustained climatic stress. As aridification intensifies across dryland and Mediterranean-climate regions (Gebrechorkos et al., 2025), understanding how agricultural WUE responds to different dimensions of water deficit becomes critical for adaptive water governance (FAO y ONU Agua, 2025; Howden et al., 2007; Wallace, 2000).

Chile provides an unusually compelling natural laboratory for this question. Since approximately 2010, central and southern Chile has experienced a persistent precipitation deficit that has been characterized as a megadrought—a multi-year dry anomaly that exceeds the interannual variability expected from modes of climate variability alone (Garreaud et al., 2017, 2020). The megadrought has reduced annual precipitation by 20-40% relative to the twentieth-century mean, depleted streamflows, and lowered groundwater levels across the country's most productive agricultural zones (Boisier et al., 2018). Parallel to precipitation reduction, atmospheric evaporative demand has intensified as warming has elevated vapor pressure deficit (VPD), compounding water stress beyond what precipitation-only indices capture (Li et al., 2023; Zambrano et al., 2025).

Despite the severity of this hydroclimatic disruption, characterized by 20-40% precipitation reductions relative to twentieth-century means, streamflow depletion, and intensified atmospheric evaporative demand through elevated vapor pressure deficit (VPD), the agricultural response, specifically in terms of WUE, has not been systematically characterized. WUE provides a systems-level signal of how efficiently agricultural land converts water into biomass under changing conditions (Hoover et al., 2023; Ito and Inatomi, 2012; Jiang et al., 2025). While Garreaud et al. (2017), Garreaud et al. (2020), and Boisier et al. (2018) document the megadrought's precipitation and hydrological impacts across Chile's productive zones, no studies have been conducted that provide a detailed analysis of cropland WUE dynamics under multidimensional aridification. Global meta-analyses reveal drought typically increases crop WUE by ~1.5% through physiological adjustments

*Corresponding author
Email addresses: francisco.zambrano@uss.cl (Francisco Zambrano), francisco.fernandez@uss.cl (Francisco Fernández), maria.molinos@uva.es (María Molinos-Senante)

(Yu et al., 2020), yet these effects vary unpredictably by crop type, drought timing, and duration without regional mechanistic breakdowns (e.g., NPP vs. ET drivers). Changes in WUE during prolonged drought may reflect multiple processes operating simultaneously: stomatal regulation under vapor pressure deficit stress, shifts in phenology, compositional changes in cropping systems, and the partial buffering of irrigated systems against precipitation deficits (Wang et al., 2024). Mediterranean irrigation studies estimate 35% potential water savings via efficient systems but rarely quantify WUE responses to combined precipitation deficits and VPD intensification in export-oriented perennial systems (Fader et al., 2016). Regional assessments in Latin America report low agricultural water utilization (35-86%) but fail to disentangle drought-specific drivers or crop-composition effects on sensitivity (Mekonnen and Hoekstra, 2011). This leaves critical gaps in understanding how Chile's export-oriented perennial horticulture responds to sustained megadrought conditions.

Agricultural crop composition is likely to modulate the WUE response to aridification. Perennial fruit crops (vineyards, orchards), which dominate the high-value export agriculture of central Chile, have different water use strategies compared with annual grain and forage crops. Perennials maintain year-round root systems and may sustain higher net primary production (NPP) under deficit conditions through deep root access, whereas annuals experience sharper productivity collapses once critical thresholds are breached (Chakraborti et al., 2023; Davis et al., 2017). The degree to which crop composition moderates WUE sensitivity to aridification signals is investigated here using agricultural census data linked to watershed-level WUE and drought records.

A key conceptual contribution of this paper is to treat aridification as a multi-process phenomenon rather than a single drought signal. Previous analyses have often used a single index, typically a precipitation-based measure, to characterize drought impacts on vegetation. However, SPEI (Standardized Precipitation-Evapotranspiration Index, Vicente-Serrano et al. (2010)) captures the combined effect of precipitation deficits and elevated atmospheric demand, SPI (Standardized Precipitation Index, Mckee et al. (1993)) isolates precipitation deficits, and EDDI (Evapoarative Demand Drought Index, Hobbins et al. (2016), McEvoy et al. (2016)) captures anomalies in atmospheric evaporative demand independently of precipitation. Whether WUE responds differently to these distinct aridification dimensions has not been established for Chilean agriculture. A methodologically distinctive feature of this study is the use of a paired-census quasi-experimental design to disentangle structural crop-composition effects from drought-driven land-use adaptation. By comparing crop-composition-sensitivity relationships estimated from the 2007 (pre-drought) and 2021 (post-drought)

agricultural censuses, and by fitting spatial error models that account explicitly for the geographic clustering of crop systems alongside aridification exposure, the study can assess whether elevated WUE-drought sensitivity in particular watershed types reflects an enduring structural property of those crop systems or a post-drought artefact of compositional change. This integration of paired-census design with spatial statistical inference, rather than treating OLS crop-composition coefficients as causally independent, constitutes the primary methodological contribution of the study alongside its multi-dimensional aridification framework.

This paper addresses the following primary question: How does agricultural WUE respond to different dimensions of aridification during the Central Chile Megadrought? Secondary questions ask: (i) Do zNPP (NPP z-score) and SETI (Standardized Evapotranspiration Index) trends reveal whether observed WUE change is driven primarily by declining vegetation productivity or by changes in actual evapotranspiration (ET)? (ii) Did WUE undergo a structural break coincident with megadrought onset around 2010? (iii) Which long-term aridification signal, SPEI, SPI, or EDDI, explains the greatest share of WUE variability? (iv) Does crop composition modulate WUE sensitivity to aridification? (v) Are WUE responses spatially clustered across Chilean watersheds?

2. Data and Methods

2.1. Study area

Continental Chile extends from approximately 17°S to 56°S, encompassing some of the world's most extreme latitudinal climate gradients within a single country (Aceituno et al., 2021). The northern Atacama region is hyperarid; the semi-arid Norte Chico (approximately 26°S-32°S) transitions into the Mediterranean-climate zone of central Chile (32°S-38°S), which concentrates the majority of the country's irrigated agriculture, viticulture, and fruit export production. South of the Biobío River (~38°S), a temperate humid zone supports rainfed cereal and forage production transitioning to temperate rainforests further south (Figure 1).

The megadrought has most severely affected the 30°S-42°S band, where precipitation deficits of 25-45% relative to the twentieth-century mean have persisted since 2010 (Boisier et al., 2018; Garreaud et al., 2020). The study uses watershed-level spatial units based on the Chilean National Water Authority (DGA, General Directorate of Water) hydrological boundaries, which provide physically meaningful aggregation units and align with the country's water allocation governance framework (Rivera et al., 2016).

2.2. WUE data

Annual cropland WUE expressed in $g \cdot C \cdot kg^{-1} H_2O \cdot^{-1}$, is defined as:

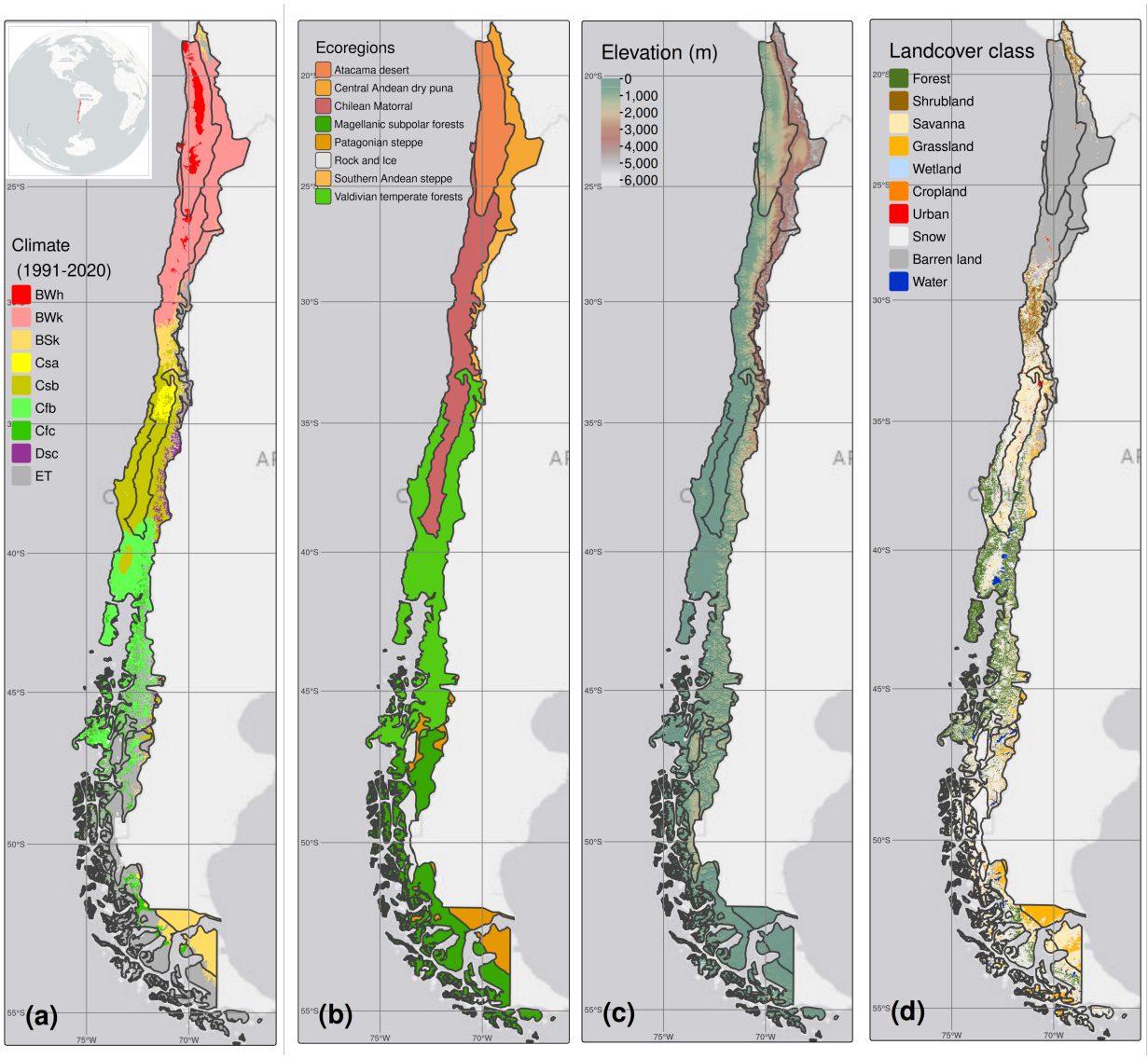

Figure 1: Climate, topography, and land cover classes across continental Chile. Koppen-Geiger climate classes (a), ecoregions (b), topography (c), and persistent land cover classes (> 80%) for 2001-2023 (d) across continental Chile. Reproduced from Zambrano et al. (2025) under CC BY 4.0 license.

$$WUE = \frac{NPP}{ET}$$

It was obtained from the global cropland WUE dataset of Jiang et al. (2025), which provides 1-km grid annual rasters for 2001-2020 derived specifically for agricultural areas. NPP was estimated using an improved Evaporative Fraction Light-Use Efficiency (EF-LUE) model driven by ERA5-Land reanalysis meteorology (temperature, solar radiation, vapour pressure deficit; bilinearly resampled from the native ~9 km resolution to 1 km as described in Jiang et al. (2025)), GLASS fAPAR and LAI (500 m, 8-day; interpolated to daily), and cropland distribution from ESA CCI-LC land cover (300 m, aggregated to 1 km). The EF-LUE model parameterises stomatal water stress via an evaporative fraction term calibrated against FLUXNET2015 flux tower observations across multiple Köppen-Geiger climate zones. Annual NPP was computed as:

$$NPP = 0.8 \times \sum_{d} GPP_d - \sum_{d} MR_d$$

where MR_d is temperature-dependent maintenance respiration of leaves and fine roots. ET was sourced from the ETMonitor product (1 km, daily, Hu and Jia (2015)), which integrates energy balance, water balance, and plant physiological processes and was validated against flux towers with correlation > 0.75. Rasters were cropped to Chile's extent (76°W-66.24°W, 56.54°S-17.49°S), then monthly, and annual mean WUE was extracted per watershed by spatial averaging. The 20-year time series (2001-2020) spans a pre-megadrought reference period (2001-2009) and the megadrought period (2010-2020).

WUE values were aggregated as arithmetic means across cropland pixels within each watershed boundary (Hoover et al., 2023; Jiang et al., 2025).

2.3. Drought drivers and WUE mechanistic components

The variables used in this study serve two analytically distinct roles. Drought drivers (SPEI, SPI, EDDI) characterize the external aridification forcing imposed on agricultural systems. WUE mechanistic components (zNPP, SETI) track the internal responses within the WUE identity, representing the numerator (NPP) and denominator (ET) separately, and are therefore not treated as additional drought indices.

2.3.1. *Aridification drivers*

Three complementary drought indices were used to characterize distinct dimensions of aridification, following the framework established in AghaKouchak et al. (2015), Gebrechorkos et al. (2023), and Zambrano et al. (2025):

SPEI (Standardized Precipitation-Evapotranspiration Index, 36-month scale) represents the primary aridification driver. SPEI captures the hydroclimatic balance by incorporating both precipitation inputs and atmospheric evaporative demand into a standardized anomaly, making it sensitive to the combined effect of precipitation deficit and VPD intensification that characterizes the megadrought (Li et al., 2023; Zambrano et al., 2025). SPEI was calculated from ERA5-Land monthly precipitation, and ET was calculated based on FAO-56 Penman-Monteith reference evapotranspiration following Vicente-Serrano et al. (2010).

SPI (Standardized Precipitation Index, 36-month scale) isolates precipitation deficits, providing a comparison signal that reflects the purely pluviometric dimension of drought without evaporative demand effects (Mckee et al., 1993).

EDDI (Evaporative Demand Drought Index, 36-month scale) characterizes anomalies in atmospheric evaporative demand independently of precipitation, thereby capturing the thermally driven component of aridification (Hobbins et al., 2016; McEvoy et al., 2016). The EDDI implementation follows a sign convention aligned with SPEI and SPI: positive values indicate below-normal evaporative demand (wet-like conditions) and negative values indicate above-normal demand (drought-like conditions). This convention inverts the original Hobbins et al. (2016) polarity and allows direct cross-index comparison with a shared interpretation (negative = drought).

All three indices were computed at the 36-month accumulation scale to capture long-term signals of aridification (Zambrano et al., 2025), regularly associated with hydrological impacts. Monthly values were extracted per watershed polygon and aggregated to annual means before analysis.

2.3.2. *WUE mechanistic components*

Two variables were incorporated to decompose WUE variability in terms of the identity WUE = NPP/ET, providing insight into whether observed WUE changes are driven by the productivity (NPP) or water use (ET) side of the ratio.

zNPP (z-score NPP) tracks the NPP numerator of WUE directly. Annual NPP estimates from

MOD17A3HGF (MODIS Terra, 500 m, Collection 6.1) were z-score standardised within the 2001-2020 reference period, yielding an anomaly series that reflects interannual variability in vegetation productivity relative to the historical mean.

SETI-36 (Standardized Evapotranspiration Index, 36-month scale) captures multi-year anomalies in actual evapotranspiration relative to the historical baseline, representing the ET denominator of WUE. Drought-induced reductions in actual ET reflect the combined effect of stomatal closure, reduced soil water availability, and phenological shifts. The imbalance between EDDI (atmospheric evaporative demand) and SETI (actual evapotranspiration) identifies watersheds where potential demand increasingly exceeds actual water use, a signal of progressive vegetation-atmosphere decoupling and physiological water stress. SETI was derived from MOD16A2GF (MODIS Terra, 500m 8-day, Collection 6.1) actual evapotranspiration data (Running et al., 2021). Because zNPP (MOD17A3HGF) and SETI (MOD16A2GF) are derived from products independent of the ETMonitor/EF-LUE pipeline used by Jiang et al. (2025) to construct the WUE rasters, this mechanistic decomposition functions as a cross-product consistency check rather than an exact algebraic decomposition of the WUE numerator and denominator.

2.4. Agricultural census data

Crop composition data were obtained from two Chilean Agricultural and Forestry Censuses: the VII Census (2007, pre-drought baseline) (INE, 2007) and the VIII Census (2020-2021, endpoint) (INE, 2021). Both censuses report cultivated area (ha) by crop category and management type (irrigated/rainfed) at commune level. Crop categories included: cereals, legumes and tubers, industrial crops, vegetables and aromatics, fruit trees, vineyards and pisco grapes, cut flowers, seed crops, nurseries, and forage crops. Categories were harmonised across census editions to ensure comparability.

Raw census data were processed to assign commune identifiers by normalizing names and cross-referencing with spatial boundary databases, including manual correction of combined entries for communes grouped for statistical confidentiality. Crop areas were preserved separately by irrigation condition (irrigated, rainfed) as reported directly in the census. Where the irrigation split was not reported directly, it was imputed from subsidiary files using residual ratios and flagged accordingly. Of the 3,807 crop-category records in the 2007 census long-format dataset, 2,535 (66.6%) used imputed irrigation splits; the 2021 census had no imputed records (all irrigation splits directly reported). Imputed values preserve national agricultural totals but may misallocate irrigation at the individual commune level, potentially introducing attenuation bias in the percentage irrigated area regression coefficient for the 2007 analysis. Given that the 2007 baseline is used

only for directional consistency checks rather than primary inference, this limitation does not affect the main crop composition results. For the 2021 analysis, which underpins the primary SEM results, the irrigated area share variable is derived entirely from directly reported data. Commune-level data were spatially aggregated to watershed level using area-weighted means via a spatial join between commune boundaries and watershed polygons. Each watershed therefore receives a crop composition vector reflecting the agricultural structure of the communes it contains.

From the per-watershed crop areas, the following proportional indicators were derived:

- *pct_fruits*: proportion of area under fruit trees
- *pct_vineyards*: proportion under vineyards and pisco grapes
- *pct_cereals*: proportion under cereals
- *pct_vegetables*: proportion under vegetables and aromatics
- *pct_forages*: proportion under forage crops
- *pct_irrigated*: irrigated share of total agricultural area (irrigated / (irrigated + rainfed)), reflecting the buffering capacity of irrigation infrastructure against precipitation deficits

Three functional aggregates were computed: perennial horticultural crops (*pct_perennials* = pct_fruits + pct_vineyards), annual cropland (*pct_annuals* = pct_cereals + pct_vegetables), and forage/pasture (*pct_forage* = pct_forages). Dominant crop type was assigned to each watershed using a 40% area threshold: if any functional group exceeded 40% of total agricultural area, the watershed was classified accordingly; otherwise it was classified as mixed.

2.5. Statistical analyses

2.5.1. Trend analysis

Mann-Kendall trend tests and Sen's slope estimates were computed per watershed using the annual WUE time series (2001-2020), which accounts for autocorrelation through prewhitening. Equivalent analyses were performed for zNPP trends, SETI trends, and atmospheric evaporative demand (EDDI) to provide comparative multi-variable context.

2.5.2. Structural break detection

The Pettitt test (Pettitt, 1979) was applied to the annual WUE series of each watershed to detect the most probable year of a shift in the mean level. The Pettitt test is a non-parametric rank-based method that does not require distributional assumptions and is widely used for hydrological change-point detection.

Benjamini-Hochberg (BH) false-discovery-rate (FDR) correction was applied to Pettitt structural break p-values (76 simultaneous watershed-level tests). Watersheds were classified by: (i) significance of the detected break ($p < 0.05$), and (ii) proximity to megadrought onset, defined as break years within ±2 years of 2010 (i.e., 2008-2012).

2.5.3. Before/after comparison

Mean WUE was computed separately for the pre-megadrought (2001-2009) and megadrought (2010-2020) periods per watershed. The difference $\Delta WUE = WUE_{post} - WUE_{pre}$ was mapped spatially. Wilcoxon signed-rank tests (paired by spatial unit) tested the significance of the mean shift at each spatial aggregation level. Distributions were visualized as violin-boxplot combinations faceted by ecoregion, using the WWF Terrestrial Ecoregions of the World classification (Dinerstein et al., 2017) to stratify results by ecological context.

2.5.4. WUE-aridification relationships

Spearman rank correlations (ρ) were computed between annual WUE and each of the three indices (SPEI, SPI, EDDI), applied per watershed across the 20-year time series. Per-watershed Spearman correlation and OLS regression results are reported without FDR correction, as each watershed p-value describes a distinct independent time series rather than constituting a family of tests on the same null hypothesis. Contemporaneous linear regressions (WUE ~ Index) were fitted per watershed to estimate the slope coefficient, which we interpret as the local sensitivity of WUE to each aridification signal ($Sensitivity = \Delta WUE / \Delta Index$). Spearman ρ values were mapped spatially and the mean ρ across watersheds was plotted as a function of each index. Sensitivity maps were produced for SPEI as the primary index.

A two-way fixed-effects panel regression model was estimated:

$$WUE_{it} = \beta \cdot Index_{it} + \mu_i + \tau_t + \varepsilon_{it} \tag{1}$$

where μ_i represents watershed fixed effects and τ_t represents year fixed effects, thereby controlling for unobserved time-invariant differences among watersheds and common annual shocks. An interaction model was additionally estimated to test whether within-watershed WUE–drought sensitivity changed after megadrought onset:

$$WUE_{it} = \beta_1 \cdot Index_{it} + \beta_2 \cdot Index_{it} \times \mathbb{1}(year \geq 2010) + \mu_i + \tau_t + \varepsilon_{it} \tag{2}$$

2.5.5. Spatial dependence analysis

Moran's I was computed for WUE trend slope, Pettitt break year, and R^2 of the WUE-SPEI relationship, using queen contiguity spatial weights. Getis-Ord Gi* local statistics were computed for WUE trend slope to identify spatial hotspots (Gi* > 1.96) and coldspots (Gi* < -1.96) at the 95% significance level. Queen contiguity was used as the primary weighting scheme because it preserves physical adjacency between watershed polygons.

2.5.6. Crop composition and WUE sensitivity

The per-watershed OLS slope of WUE regressed on SPEI ($\Delta WUE/\Delta SPEI$) was joined with census-derived crop composition data, and a multiple OLS regression was fitted:

$$\begin{aligned} Sensitivity_i = \beta_0 + \beta_1 \cdot pct\_fruits_i + \beta_2 \cdot pct\_vineyards_i + \beta_3 \cdot pct\_cereals_i \\ + \beta_4 \cdot pct\_vegetables_i + \beta_5 \cdot pct\_irrigated_i + \varepsilon_i \end{aligned} \tag{3}$$

Forage and pasture proportions (*pct_forages*) served as the reference category and were omitted from the model to avoid the dummy variable trap; regression coefficients therefore express the change in WUE sensitivity relative to a watershed whose agricultural area is entirely under forage or pasture. Variance inflation factors (VIF) were computed to verify the absence of harmful multicollinearity (threshold: VIF > 5). The variable *pct_irrigated* was included as a covariate to control for the buffering effect of irrigation access on the WUE-drought relationship. Because WUE trends exhibit strong spatial autocorrelation (Moran's I $=$ 0.627), Moran's I was also computed on the OLS residuals using queen-contiguity spatial weights; where residuals were spatially autocorrelated ($p < 0.05$), a spatial error model was estimated and reported alongside OLS results.

A sensitivity regression using pre-drought (2007) census proportions as predictors was also estimated to address temporal confounding concerns: if results are directionally consistent with the 2021 regression, the crop composition-sensitivity relationship can be interpreted as a structural property rather than an artefact of drought-driven adaptation (see Section 4.3 and Supplementary Figure S-1).

2.6. Software

All statistical analyses and spatial processing were conducted in R (v4.5.2; R Core Team (2025)). Raster operations and spatial aggregation used `terra` (v1.8.54; Hijmans (2025)). Vector geometries and spatial joins used `sf` (v1.0.23; Pebesma (2018), Pebesma and Bivand (2023)). Spatiotemporal array operations used `stars` (v0.6.8; Pebesma and Bivand (2023)). Mann-Kendall trend tests and Sen's slope estimation with prewhitening used `modifiedmk` (v1.6; Patakamuri and O'Brien (2021)) and `trend` (v1.1.6; Pohlert (2023)). Spatial autocorrelation (Moran's I, Getis-Ord Gi*) and spatial weight matrices used `spdep` (v1.4.1; Bivand and Wong (2018)). Spatial Error Model was made using `{spatialreg}` (Bivand et al., 2021). Panel regression with fixed effects used `plm` (Croissant and Millo, 2008). Variance inflation factors used `car` (v3.1.3; Fox and Weisberg (2019)). General-purpose data manipulation and reshaping used `tidyverse` (v2.0.0; Wickham et al. (2019)), including `dplyr`, `tidyr`, `readr`, `stringr`, `purrr`, and `lubridate`. Thematic maps used `tmap` (v4.2; Tennekes (2018)). Statistical graphics used `ggplot2` (v3.5.2; Wickham (2016)). Multi-panel figure layout used `patchwork` (v1.3.1; Pedersen (2025)).

3. Results

3.1. Long-term WUE trends

Trend analysis across n = 76 Chilean agricultural watersheds with complete WUE data revealed spatially heterogeneous WUE dynamics over the 2001-2020 period (Figure 2). WUE trends followed a predominantly negative pattern across the Mediterranean-climate zone of central Chile (approximately 30°S-35°S), consistent with the onset and intensification of the megadrought.

Decomposing WUE trends into their mechanistic components, zNPP representing the NPP numerator and SETI representing the ET denominator, reveals the distinct contributions of productivity decline and evapotranspiration change to the observed WUE dynamics. zNPP trends exhibited strong spatial covariance with WUE, with negative anomalies concentrated in the same central Mediterranean watersheds, indicating that NPP suppression is the primary driver of WUE deterioration in those zones (Garreaud et al., 2017; Zambrano et al., 2025). SETI trends showed more spatially complex patterns: watersheds where actual ET declined less steeply than NPP correspond to WUE decline, while watersheds where ET reduction exceeded NPP reduction show stable or improving WUE.

Declining WUE in the Mediterranean zone is thus driven primarily by NPP suppression, while ET responses are spatially heterogeneous and modulated by irrigation access and crop type.

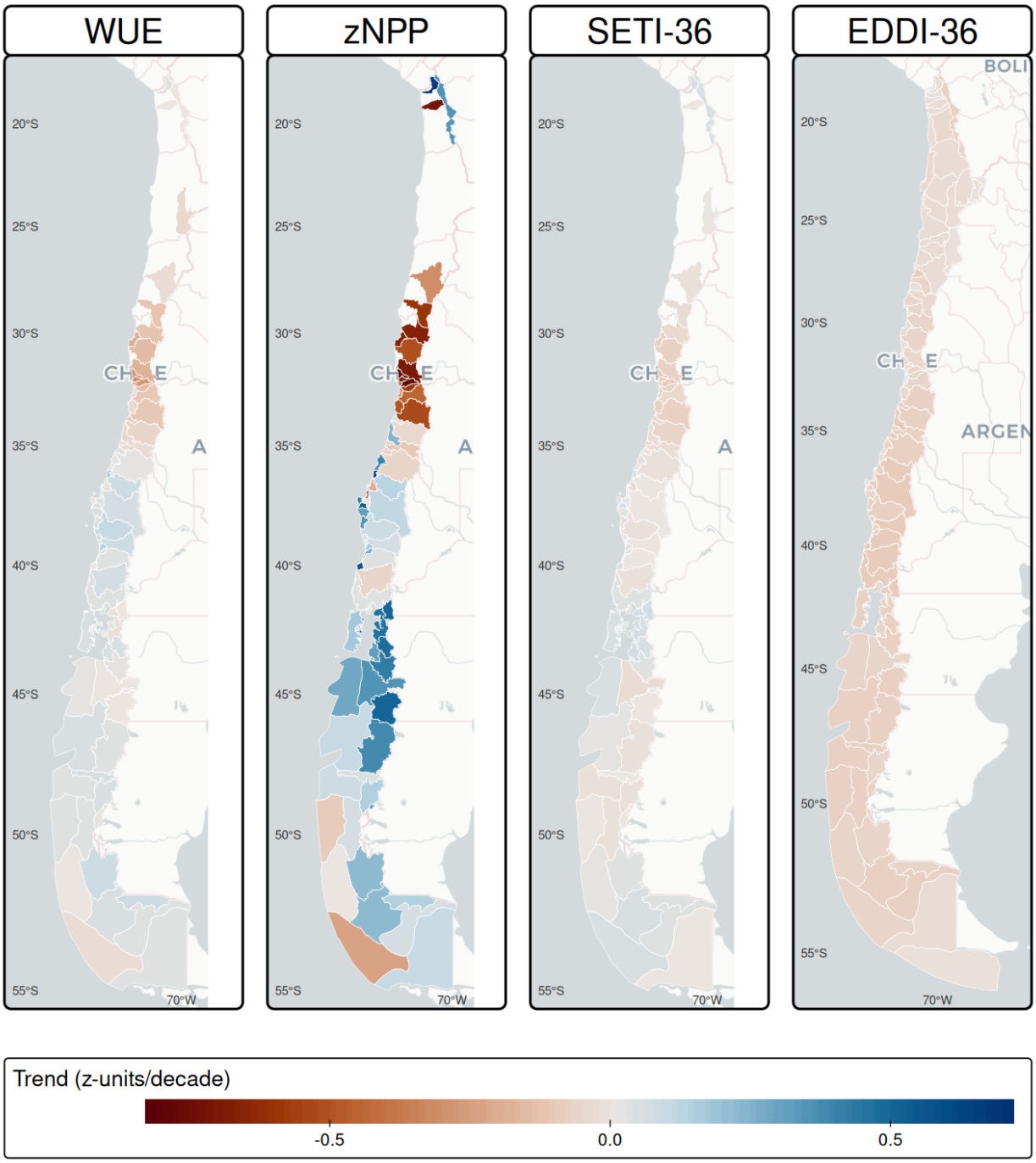

Figure 2: Spatial distribution of long-term trends in WUE, zNPP (NPP anomaly), SETI-36 (long-term ET anomaly), and EDDI-36 (long-term atmospheric evaporative demand) across Chilean watersheds (2001-2020). Trend magnitudes are expressed as z-score standardized Sen's slope estimates.

3.2. Structural breaks in WUE

The Pettitt test detected statistically significant structural breaks ($p < 0.05$) in 17 of 76 Chilean watersheds (22.4%). Of these 17 raw-significant breaks, 12 (71%) occurred within ±2 years of 2010 (the recognized onset of the megadrought) suggesting that the megadrought is temporally associated with structural shifts in WUE dynamics in a subset of watersheds (Figure 3 a). After applying Benjamini-Hochberg false-discovery-rate (FDR) correction across all 76 per-watershed tests, none of the breaks survived at the 0.05 threshold (all adjusted $p > 0.05$), reflecting the limited power of individual non-parametric tests applied across spatially correlated watersheds with only 20 annual observations each. The geographic concentration of near-2010 breaks in the central Mediterranean zone — precisely where the megadrought's hydroclimatic footprint is strongest — provides qualitative corroboration that these detections are not randomly distributed in space, even if they cannot be treated as statistically independent given the documented spatial autocorrelation in WUE dynamics (Moran's I for break year = 0.164, $p = 0.011$).

Spatially, megadrought-proximate break years were concentrated in the central and north-central Mediterranean zone, supporting the interpretation that the megadrought represents a structural discontinuity in agricultural water use efficiency for those regions. Watersheds in the extreme north (hyperarid Atacama) and the wet south showed either no significant breaks or break years unrelated to the 2010 megadrought onset, consistent with the spatial footprint of the megadrought as documented by Garreaud et al. (2020) and Boisier et al. (2018).

3.3. WUE before and after the megadrought

Comparison of mean WUE between the pre-megadrought (2001-2009) and megadrought (2010-2020) periods revealed a predominantly negative ΔWUE across central Chilean watersheds, indicating that the megadrought period was associated with reduced agricultural water use efficiency relative to the reference period (Figure 3 b). The spatial pattern of ΔWUE closely mirrors the megadrought's hydroclimatic footprint, with the largest negative shifts concentrated in Mediterranean-climate watersheds where the precipitation deficit has been most severe.

The aggregate Wilcoxon signed-rank test comparing pre-megadrought (2001-2009) and megadrought (2010-2020) mean WUE across all 76 watersheds did not reach statistical significance ($p = 0.330$). This aggregate non-significance reflects the spatial heterogeneity of WUE responses across ecologically diverse watersheds: pooling Mediterranean-climate zones (where declines are concentrated) with southern humid zones (where WUE responses are weaker or mixed) attenuates the overall effect. Ecoregion-stratified Wilcoxon tests

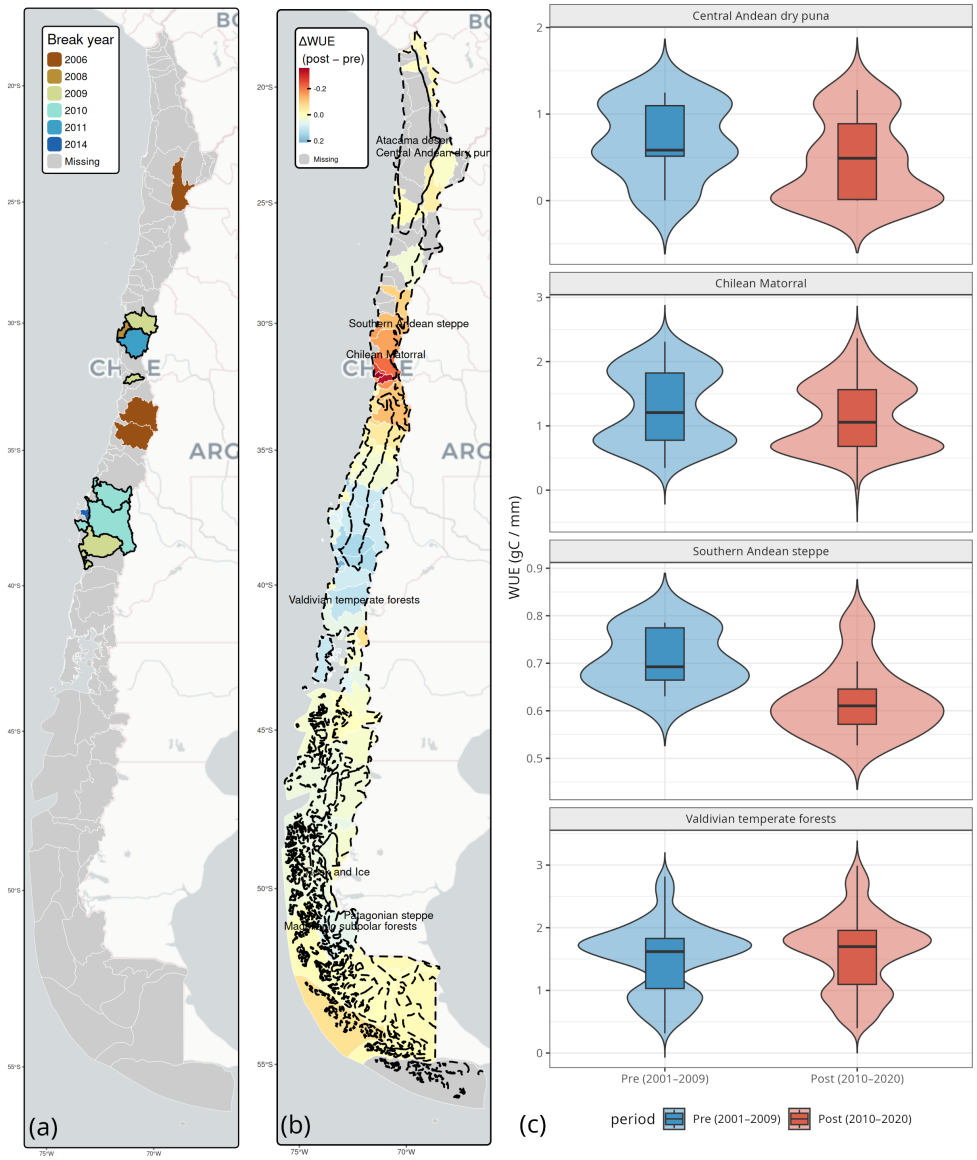

Figure 3: (a) Spatial distribution of structural break years in annual WUE per watershed, detected by the Pettitt test (significant breaks at $p < 0.05$). Watersheds with break years within ± 2 years of the megadrought onset (2010) are highlighted with bold borders, indicating megadrought-proximate structural change. Non-significant breaks are shown in grey. (b) Spatial map of WUE change between the megadrought period (2010-2020) and the pre-megadrought period (2001-2009) ($\Delta WUE = WUE_{post} - WUE_{pre}$) per watershed. Positive values (blue) indicate watersheds where mean WUE increased; negative values (red) indicate WUE decline. Ecoregion boundaries (dashed lines) are overlaid for ecological context. (c) Violin-boxplot distributions of annual WUE for the pre-megadrought (blue, 2001-2009) and megadrought (red, 2010-2020) periods, stratified by ecoregion. Each panel corresponds to one ecoregion; y-axes are free-scaled.

(Supplementary Table S-2) confirmed that the WUE shift was strongest in the Chilean Matorral ecoregion, the primary Mediterranean-climate agricultural zone, with a Hodges-Lehmann median difference of −0.132 $g \cdot C \cdot kg^{-1}H_2O\cdot^{-1}$ (95% CI: −0.203 to −0.073; $p < 0.001$), consistent with the documented hydroclimatic footprint. Violin-boxplot distributions stratified by ecoregion (Figure 3 c) confirm that the strongest negative WUE shifts are concentrated in central Chile's Mediterranean-climate watersheds, while southern transitional zones show more variable or positive responses.

3.4. WUE responses to aridification signals

Spearman correlation analysis revealed positive associations between annual WUE and SPEI across most Chilean watersheds (Figure 4), indicating that wetter years (higher SPEI) are generally associated with higher WUE, while drought years (lower SPEI) correspond to lower WUE. The strength of this relationship varied spatially and by drought index.

SPEI and SPI showed broadly similar spatial correlation patterns with WUE across Chilean watersheds, with mean temporal R^2 of 0.181 (SPEI) and 0.172 (SPI), a difference of only 0.009 that was not statistically significant in paired comparisons across per-watershed R^2 values (Wilcoxon signed-rank test: $p = 0.504$, median difference = 0.002). Both SPEI and SPI significantly outperformed EDDI in temporal explanatory power (mean $R^2 = 0.113$; SPEI vs. EDDI: $p < 0.001$, median difference = 0.064). This result does not support a claim of SPEI superiority over SPI for this dataset; rather, it suggests that incorporating atmospheric evaporative demand (through SPEI's PET term) provides negligible additional predictive power over precipitation-alone (SPI) for annual WUE variability at the 36-month accumulation scale. EDDI showed correspondence to the correlations with SPI/SPEI, although there were some differences observed in the central and southern regions of the country, which aligns with the more complex role of atmospheric demand anomalies across various ecological contexts.

3.5. Panel regression: spatial versus temporal WUE-drought relationships

A two-way fixed-effects panel regression model (Equation 1), controlling for watershed-level time-invariant differences (μ_i) and common annual shocks (τ_t), yielded non-significant coefficients for all three drought indices when estimated across all 76 watersheds: SPEI ($\beta = -0.009$, SE = 0.017, $\rho = 0.589$), SPI ($\beta = -0.015$, SE = 0.016, $\rho = 0.363$), and EDDI ($\beta = -0.002$, SE = 0.014, $\rho = 0.860$). In contrast, zNPP was strongly significant ($\beta = 0.124$, SE = 0.016, $\rho < 0.001$).

This contrast indicates that the WUE-drought index relationship is primarily driven by *between-watershed*

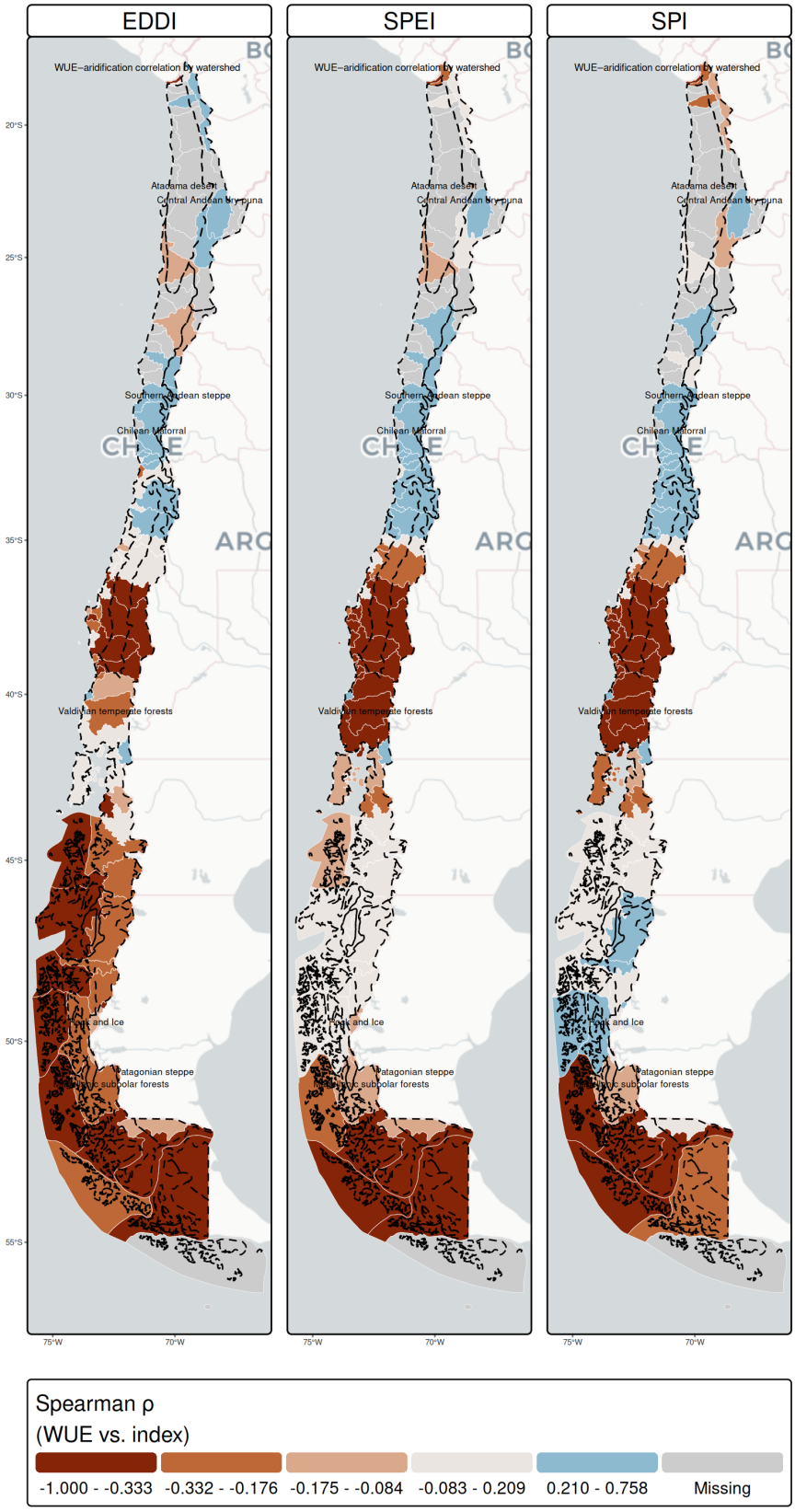

Figure 4: Spatial maps of Spearman (WUE vs. drought index) per watershed, faceted by drought index (SPEI, SPI, EDDI). Diverging colour scale (blue = positive correlation, red = negative correlation).

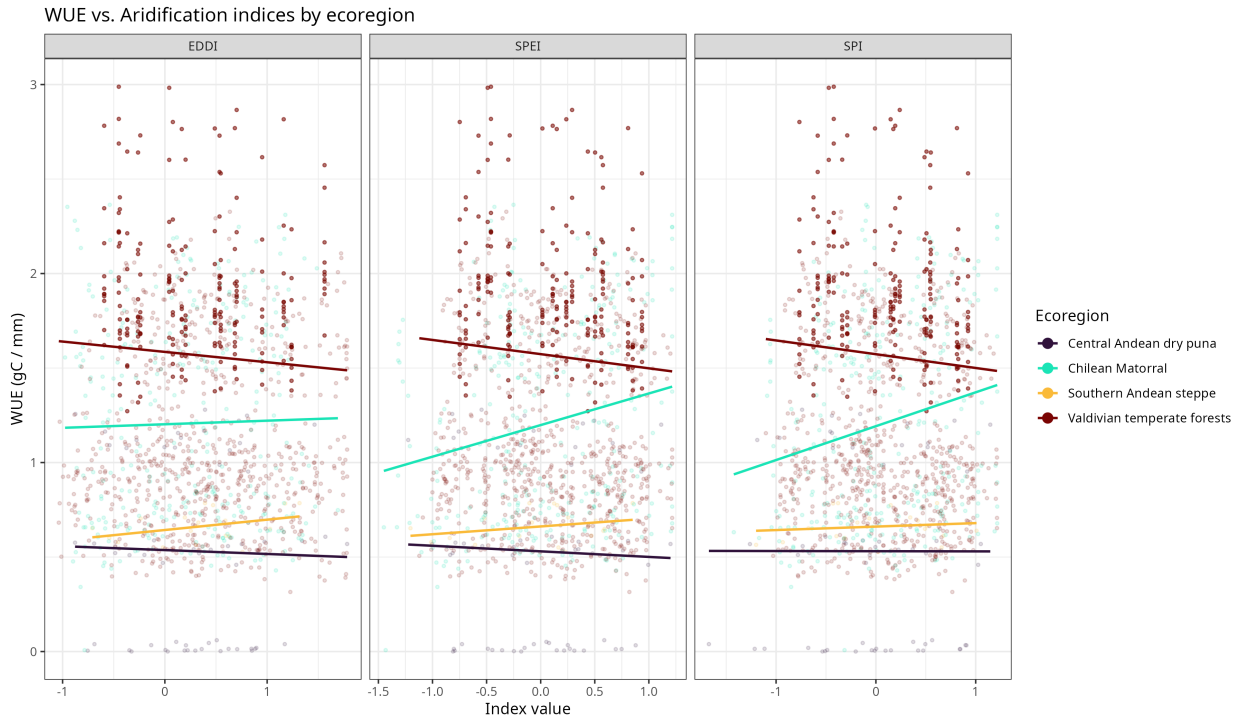

Figure 5: Scatter plots of annual WUE versus index values for SPEI, SPI, EDDI, and zNPP, stratified by ecoregion (colour). Grey line shows the overall linear fit with 95% confidence interval.

spatial differences, watersheds in drier areas structurally have both lower WUE and more negative drought index values, rather than by *within-watershed* year-to-year covariation of WUE and drought stress. The panel fixed effects absorb all time-invariant watershed characteristics (aridity zone, crop system, soil type, irrigation access), leaving only the within-watershed temporal variation to be explained. That zNPP retains significance in this design is consistent with the WUE = NPP/ET identity: as a direct measure of annual vegetation productivity, zNPP tracks the NPP component of WUE at the within-watershed annual scale. SPEI, SPI, and EDDI, by contrast, are distal aridification drivers whose association with WUE operates primarily through the chronic spatial aridity gradient — which is absorbed by watershed fixed effects.

Restricting the panel model to the Mediterranean-zone watersheds (Chilean Matorral ecoregion, n = 16), where the megadrought's hydroclimatic signal is strongest, yielded significant within-watershed WUE-drought associations for SPEI ($\beta = 0.124$, $\rho = 0.006$) and SPI ($\beta = 0.085$, $\rho = 0.012$), while EDDI remained non-significant ($\beta = 0.001$, $\rho = 0.979$). This finding confirms that the all-watershed non-significance reflects geographic dilution of the drought signal by drier northern and wetter southern watersheds rather than a genuine absence of within-watershed temporal coupling: once the analysis is restricted to the core megadrought zone, both precipitation-based indices show significant positive within-watershed WUE-drought associations.

The interaction model (Equation 2) tested whether within-watershed WUE–drought sensitivity changed structurally after megadrought onset. The SPEI interaction coefficient was marginal ($\beta = 0.079$, $\rho = 0.056$), while SPI ($\beta = 0.043$, $\rho = 0.269$) and EDDI ($\beta = -0.010$, $\rho = 0.742$) were non-significant. The marginal SPEI result suggests a modest intensification of within-watershed sensitivity to hydroclimatic balance during the megadrought period, but does not constitute strong evidence of a structural shift: the drought-period WUE decline operates predominantly through the spatial aridity gradient rather than through an intensified within-watershed temporal mechanism.

3.6. Spatial distribution of WUE sensitivity

The WUE-SPEI sensitivity map (Figure 6 a) shows the OLS regression slope ($\Delta WUE/\Delta SPEI$) per watershed. Sensitivity broadly follows the latitudinal aridity gradient. Central Mediterranean watersheds exhibited higher values than humid southern watersheds, with locally high sensitivity in perennial-dominated irrigated zones (Figure 6 c and d).

3.7. Spatial clustering of WUE trends

Moran's I statistics confirmed significant positive spatial autocorrelation in WUE trends, Pettitt break years, and WUE-SPEI R^2 values across Chilean watersheds. Moran's I for WUE trend slope was I = 0.627 ($p < 0.001$), for Pettitt break year I = 0.164 ($p = 0.011$), and for WUE-SPEI R^2 I = 0.296 ($p < 0.001$), all indicating that WUE response to the megadrought is not spatially random but exhibits strong geographic clustering. Adjacent watersheds tend to show similar trend directions, break timing, and drought sensitivity (Figure 6 b).

Getis-Ord Gi* hotspot analysis of WUE trend slopes identified coherent clusters of declining WUE (coldspots) in the central Mediterranean zone and localized clusters of increasing or stable WUE (hotspots) in transitional zones north and south of the primary drought impact corridor (Figure 6 b). The spatial clustering of WUE responses points to large-scale hydroclimatic forcing—specifically the megadrought—as the dominant driver of WUE dynamics, rather than localized management or land-use effects.

3.8. Agricultural crop composition and WUE sensitivity

The maps of dominant crop type (Figure 6 c) and perennial crop share (Figure 6 d), provide spatial context for interpreting the WUE sensitivity patterns. Integration of census-derived crop composition with WUE-SPEI sensitivity estimates (n = 75 watersheds with complete WUE, irrigation, and census data) revealed a significant positive association between perennial crop share and drought sensitivity (Figure 7),

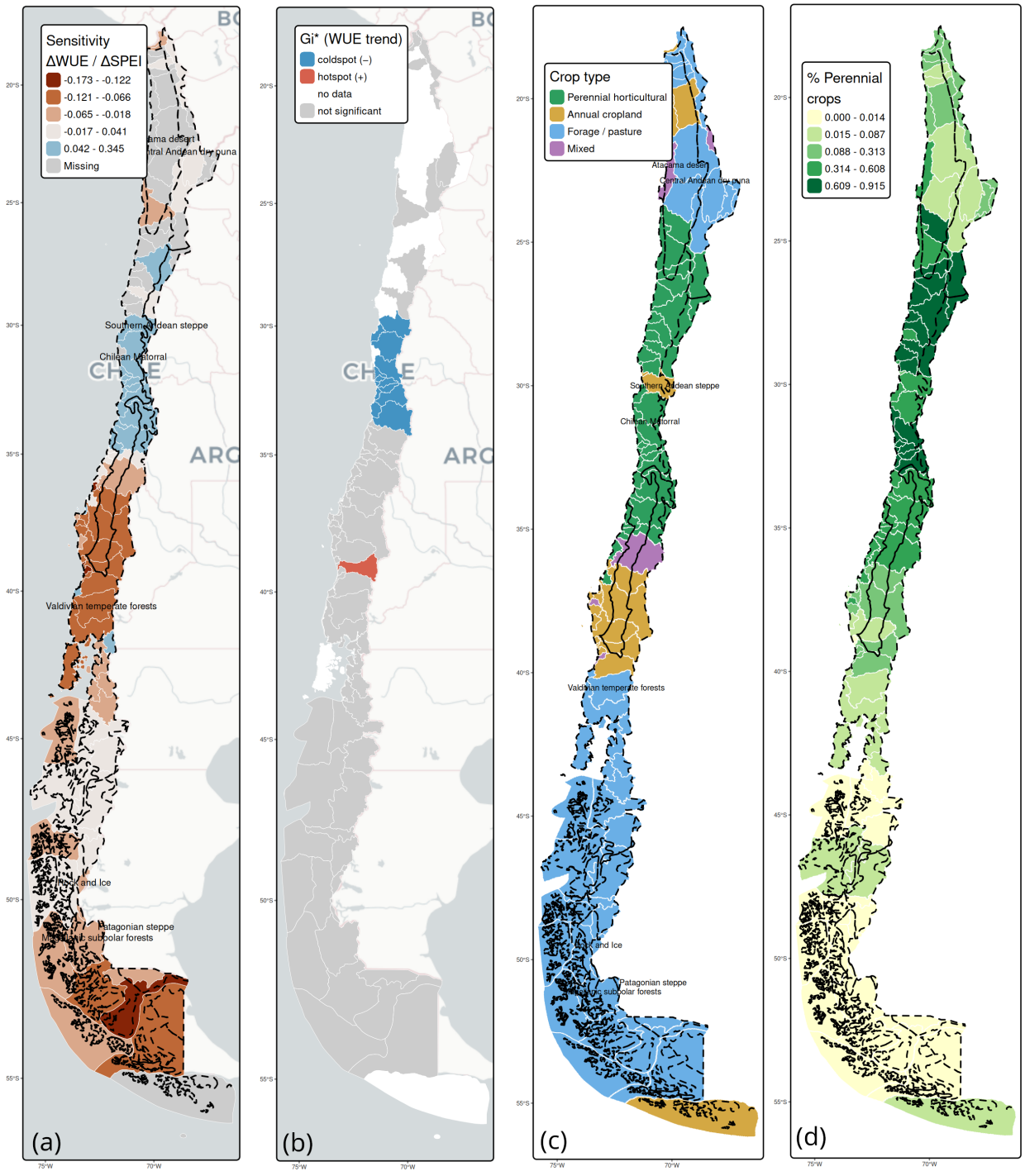

Figure 6: (a) Spatial distribution of WUE-SPEI sensitivity ($\Delta WUE/\Delta SPEI$, expressed as the OLS slope of the annual WUE ~ SPEI regression per watershed, 2001-2020). High positive values indicate strong positive WUE response to SPEI; near-zero or negative values indicate weak or inverted coupling. (b) Getis-Ord Gi* hotspot analysis of WUE trend slope across Chilean watersheds. Red watersheds are statistically significant hotspots (positive WUE trend clusters; Gi* > 1.96); blue are coldspots (negative WUE trend clusters; Gi* < -1.96); grey are not significant at the 95% level. (c) Choropleth map of dominant crop type per watershed, classified by the agricultural functional group exceeding 40% of total agricultural area (Perennial horticultural, Annual cropland, Forage/pasture, Mixed). (d) Choropleth map of perennial crop share (% of total agricultural area under fruit trees and vineyards) per watershed.

suggesting that this is a crop-system property rather than an artifact of ecoregion geography. This implies that perennial agricultural systems in Chile are more sensitive to aridification fluctuations, both benefiting more in wet years and suffering more in dry years-compared with annual crop systems. Watersheds classified as "perennial horticultural" (40% of agricultural area under fruit trees and vineyards) exhibited the highest median WUE-SPEI sensitivity, whereas "forage/pasture" watersheds showed the lowest. "Annual cropland" watersheds showed intermediate but spatially variable sensitivity, reflecting heterogeneous responses among cereal and vegetable crops.

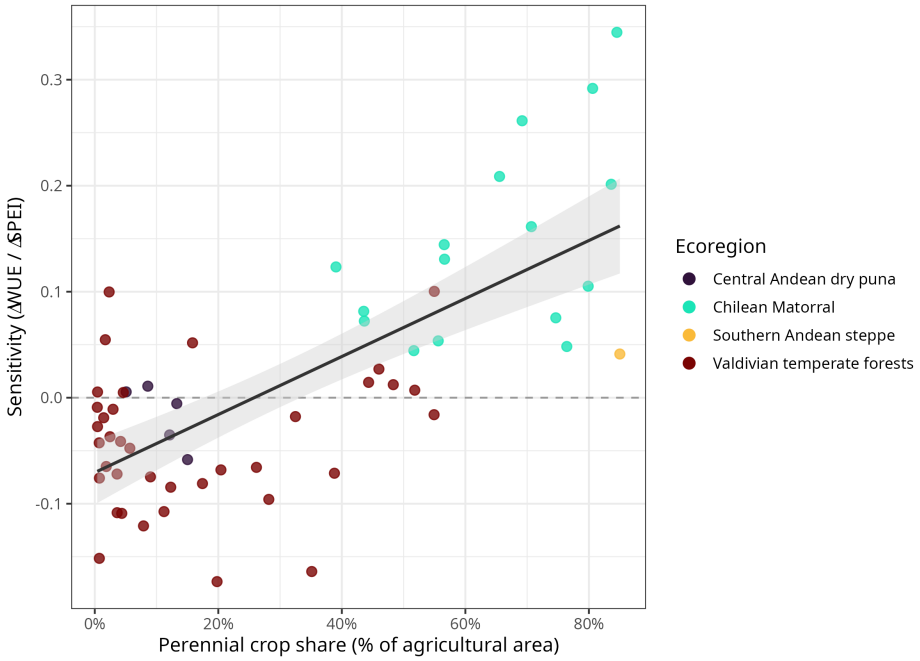

Figure 7: Scatter plot of WUE-SPEI sensitivity versus the perennial crop share (% of total agricultural area) per watershed, coloured by ecoregion, with an overall linear fit.

The multivariate OLS regression of WUE-SPEI sensitivity on 2021 crop proportions, controlling for irrigated area share, was fitted to the 75 watersheds with agricultural land, complete WUE data, and non-missing irrigation data ($R^2 = 0.576$, adj. $R^2 = 0.545$, $F(5,69) = 18.74$, $p < 0.001$, $n = 75$; Figure 8). Fruit tree proportion was the strongest positive predictor ($\beta = 0.213$, 95% CI [0.117, 0.310], $\rho < 0.001$), confirming that perennial horticultural systems are the most drought-sensitive land use type. Cereal proportion was a significant negative predictor ($\beta = -0.207$, 95% CI [−0.322, −0.093], $\rho < 0.001$), indicating that annual grain-crop watersheds exhibit substantially lower WUE-SPEI sensitivity than the forage/pasture reference category. Vineyard proportion was positive but not statistically significant (= 0.092, 95% CI [−0.105, 0.289], $p = 0.354$). Vegetables were also non-significant ($\beta = -0.056$, 95% CI [−0.205, 0.093], $\rho = 0.456$). Irrigated

area share (*pct_irrigated*) did not reach statistical significance after controlling for crop composition ($\beta = 0.046$, 95% CI [−0.032, 0.123], p = 0.241), suggesting that the irrigation-buffering effect is largely captured by the crop type variables. Forage/pasture served as the reference category (omitted). All variance inflation factors were below 5, confirming the absence of harmful multicollinearity.

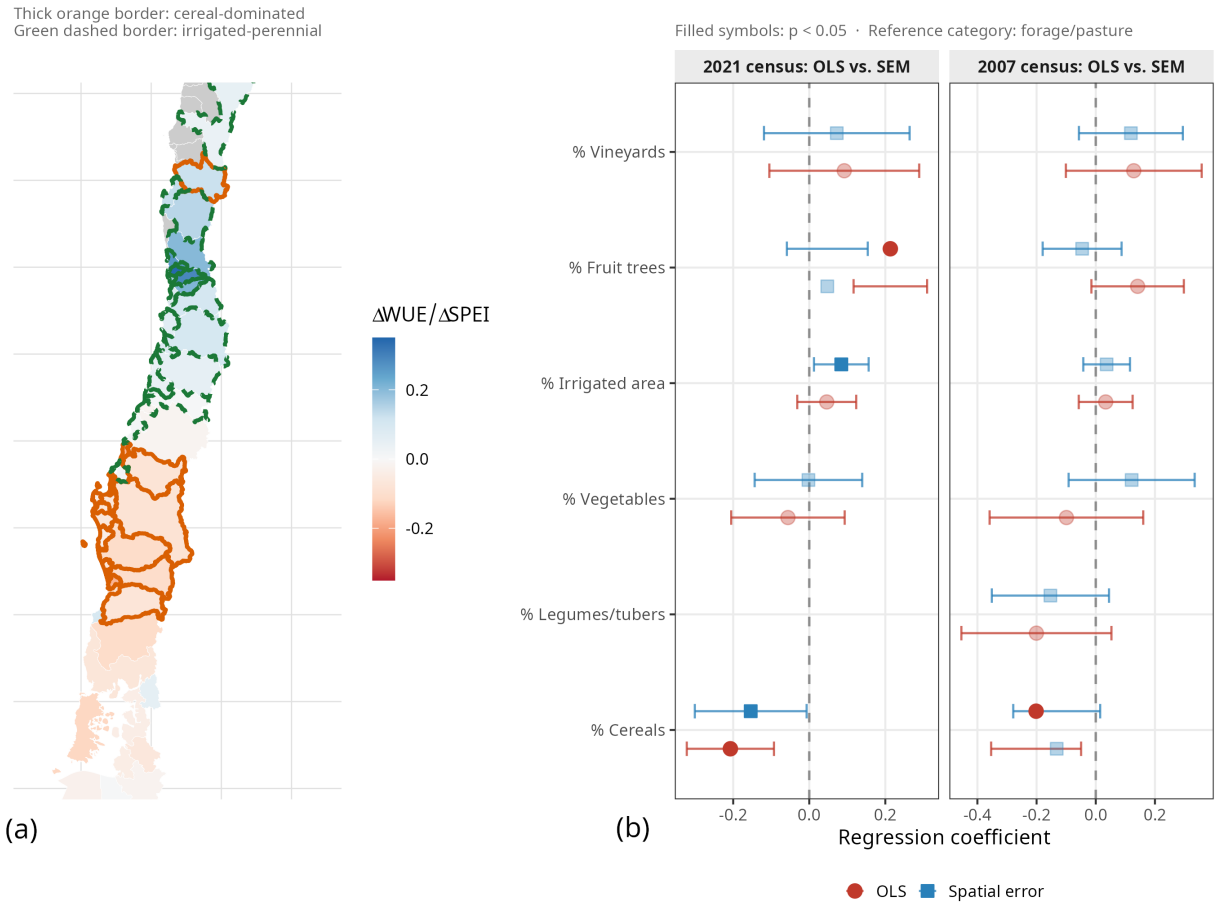

Figure 8: (a) Choropleth map of WUE–SPEI sensitivity (ΔWUE/ΔSPEI, OLS slope per watershed, 2001–2020). Thick orange borders denote cereal-dominated watersheds (Annual cropland dominant); green dashed borders denote irrigated-perennial watersheds (Perennial horticultural dominant). (b) Regression coefficients of crop-composition variables predicting WUE–SPEI sensitivity, faceted by census year. Left facet: 2021 census OLS (red circles) vs. spatial error model (blue squares); right facet: 2007 pre-drought census OLS vs. SEM. Filled symbols indicate $p < 0.05$. Reference category: forage/pasture.

Moran's I computed on OLS residuals was I = 0.309 ($p < 0.001$), indicating significant positive spatial autocorrelation in the residuals. A spatial error model (queen-contiguity weights) was therefore fitted as the primary inferential model (spatial autoregressive error parameter $\lambda = 0.615$, $\rho < 0.001$). The spatial error model partially modified the OLS conclusions: fruit tree proportion was no longer statistically significant ($\beta = 0.047$, $\rho = 0.382$), suggesting that its OLS significance was partly driven by the geographic clustering of perennial orchards in the Mediterranean zone rather than an independent crop-composition effect on

sensitivity. Cereal proportion remained a significant negative predictor ($\beta = -0.154$, $\rho = 0.040$), and irrigated area share became a significant positive predictor ($\beta = 0.084$, $\rho = 0.022$), indicating that after accounting for spatial clustering, irrigation access is associated with higher WUE-SPEI sensitivity, possibly because irrigated watersheds sustain production and thus show stronger drought coupling through the NPP component of WUE.

A pre-drought (2007) baseline regression (watershed-level, n = 75; $R^2 = 0.306$, adj. $R^2 = 0.234$, $F(7,67) = 4.23$, $p < 0.001$; Supplementary Figure S-1) was directionally consistent: cereal proportion was a significant negative predictor ($\beta = -0.202$, 95% CI [−0.354, −0.050], p = 0.010), while fruit tree proportion was positive but did not reach statistical significance at $p < 0.05$ ($\beta = 0.142$, 95% CI [−0.015, 0.298], p = 0.075). The 2007 spatial error model (= 0.731, $p < 0.001$) also showed a non-significant fruit tree coefficient ($\beta = -0.046$, p = 0.498) and a marginally non-significant cereal coefficient ($\beta = -0.132$, p = 0.078). The directional consistency of the cereal effect across census years supports a structural rather than adaptive interpretation of the crop composition–sensitivity relationship (see Section 4.3).

To assess whether the WUE-SPEI sensitivity associations are confounded by natural vegetation (matorral) contamination within the agricultural mask, natural vegetation fraction per watershed was computed from ESA CCI-LC (2016; classes 40, 120–122, 130) and added as a covariate to the spatial error model. Median natural vegetation fraction within agricultural pixels was 0.267 (range 0.00–0.60), reflecting the substantial fragmentation of the agricultural landscape in central Chile. When included in the spatial error model, the natural vegetation fraction was non-significant ($\beta = -0.017$, p = 0.810), and the primary crop composition coefficients were directionally consistent with the base model, indicating that matorral contamination does not substantially confound the WUE sensitivity associations.

To examine whether the positive WUE-SPEI sensitivity of perennial-dominated watersheds reflects the NPP numerator, the ET denominator, or both components of WUE, per-watershed OLS sensitivity slopes were computed separately for zNPP~SPEI and for SETI~SPEI (the MODIS evapotranspiration anomaly index) and then regressed on the same crop composition variables. For the NPP component (zNPP-SPEI; OLS $R^2 = 0.519$, n = 99), vineyard proportion was the strongest positive predictor (OLS: $\beta = 1.841$, $p < 0.001$; SEM: $\beta = 0.769$, p = 0.036), and cereal proportion was a significant negative predictor in OLS ($\beta = -0.614$, p = 0.016) but not in the spatial error model ($\beta = 0.017$, p = 0.953). For the ET component (SETI-SPEI; OLS $R^2 = 0.348$, n = 100), vineyard proportion was also positive (OLS: $\beta = 1.061$, p = 0.005) and cereal proportion was negative (OLS: $\beta = -0.837$, p = 0.001), but after spatial error correction, all coefficients

were non-significant (SEM = 0.668). These results indicate that the positive WUE-SPEI sensitivity of vineyard-dominated watersheds is primarily driven by greater NPP suppression under drought rather than ET maintenance, while the crop composition associations for the ET component do not survive spatial autocorrelation correction.

3.9. Cross-sectional analysis and model comparison

Cross-sectional regressions using the census year 2020 (where WUE, drought index, and crop composition are contemporaneous) confirmed the temporal patterns. Adding crop composition proportions to the cross-sectional models increased R^2 substantially for all indices: from 0.0004 to 0.432 for SPEI, from 0.078 to 0.459 for SPI, and from 0.234 to 0.431 for EDDI (Figure 9). Mean temporal R^2 (averaged across the full 2001-2020 per-watershed regressions) was 0.181 for SPEI, 0.172 for SPI, and 0.113 for EDDI. The substantially larger R^2 gains from adding crop composition in the 2020 cross-section compared with temporal models suggest that crop structure explains a greater share of the spatial distribution of drought sensitivity than of its interannual variability within each watershed. Sample sizes for each analytical step are documented in Supplementary Table S-1 (n = 75 watersheds with complete WUE, irrigation, and census data used in crop composition analyses).

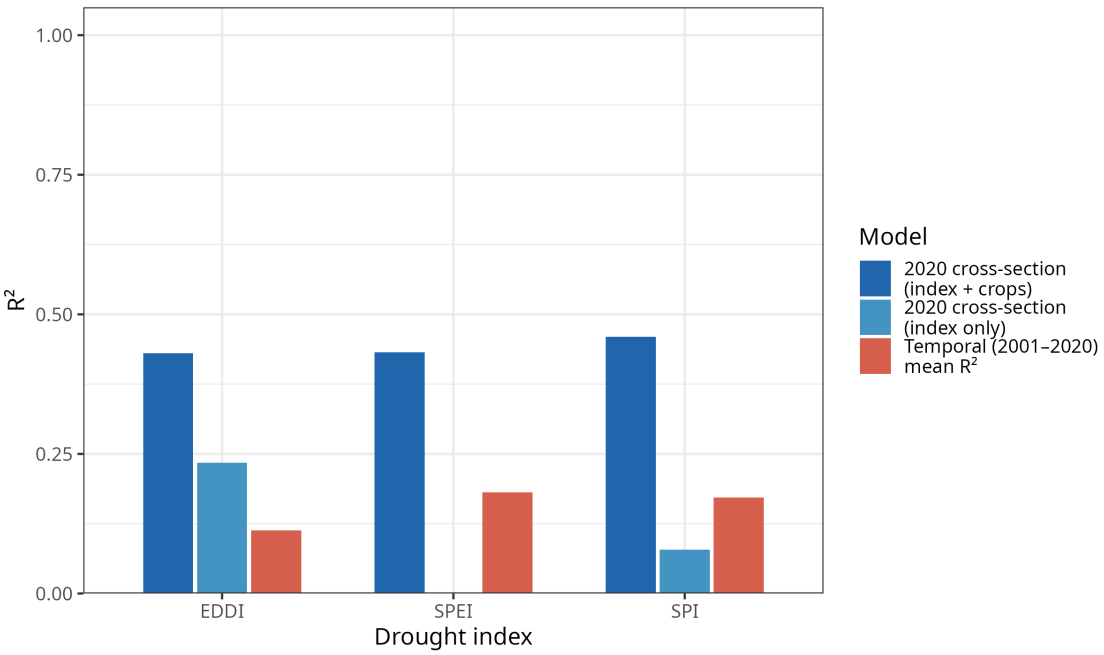

Figure 9: Bar chart comparing R^2 values across three model types for each drought index: (i) 2020 cross-sectional regression (index only: SPEI = 0.0004, SPI = 0.078, EDDI = 0.234), (ii) 2020 cross-sectional regression (index + crop proportions: SPEI = 0.432, SPI = 0.459, EDDI = 0.431), and (iii) temporal regression (mean R^2: SPEI = 0.181, SPI = 0.172, EDDI = 0.113).

4. Discussion

4.1. The megadrought as a structural driver of WUE change

The Pettitt test results indicate that 17 of 76 watersheds (22.4%) showed raw-significant structural breaks ($p < 0.05$) in WUE dynamics, with 71% of those breaks concentrated around 2010. While none survived Benjamini-Hochberg FDR correction, reflecting the limited statistical power of individual tests applied to spatially correlated watersheds with only 20 annual observations, the near-2010 concentration of raw-significant breaks is geographically coherent and consistent with the onset of the megadrought. This finding is best interpreted as evidence that WUE dynamics are *temporally associated with* the megadrought onset rather than as definitive statistical proof of a structural break: the spatial concentration of change points in the central Mediterranean zone, precisely where the megadrought's hydroclimatic footprint is strongest (Boisier et al., 2018; Garreaud et al., 2020), provides geographic corroboration. The geographic coherence of near-2010 breaks in this zone supports a megadrought-associated interpretation, though the spatial autocorrelation among watersheds (Moran's I for break year = 0.164, $p = 0.011$) means the 17 Pettitt results cannot be treated as independent observations, which precludes formal inference about temporal clustering from independence-based tests.

This finding is consistent with the broader literature on regime shifts in ecological and agricultural systems under sustained stress (Folke et al., 2004), and reinforces the interpretation of the megadrought as a transformative stress event rather than an incremental trend (Kates et al., 2012). The implications for water management are significant: if WUE has undergone a step-change downward in central Chile, agricultural water requirements per unit of production have increased, placing additional pressure on already-stressed water allocation systems (Budds, 2020; Rivera et al., 2016).

4.2. Multidimensional aridification: why index choice matters

SPEI and SPI showed statistically indistinguishable temporal explanatory power ($p = 0.504$), indicating that incorporating atmospheric evaporative demand (SPEI's PET term) provides negligible predictive gain over precipitation-alone (SPI) at the 36-month accumulation scale, likely because precipitation deficits and evaporative demand anomalies are strongly correlated over multi-year megadrought periods (Li et al., 2023; Zambrano et al., 2025). EDDI was significantly weaker than both, suggesting that atmospheric demand anomalies in isolation are less directly coupled to WUE at the watershed scale.

EDDI's distinct spatial correlation pattern indicates partially independent effects of atmospheric demand on

WUE. Semi-partial Spearman correlations (controlling for SPEI) confirmed a modest independent EDDI signal (mean partial $\rho = 0.041$ vs. unconditional $\rho = 0.069$), consistent with strong thermodynamic coupling between precipitation deficit and VPD (Li et al., 2023). The EDDI effect is therefore a statistical association rather than a causally isolated demand pathway; in irrigation-buffered watersheds, near-zero EDDI correlations reflect sustained production when water supply is maintained.

This result has practical implications for drought monitoring and agricultural water management: because SPEI and SPI show statistically equivalent explanatory power at the 36-month scale, precipitation-only monitoring (SPI) may be sufficient for characterizing annual WUE variability under conditions similar to the megadrought. However, in shorter-accumulation or sub-seasonal contexts where evaporative demand anomalies decouple from precipitation deficits, relying solely on SPI could underestimate WUE impacts in regions experiencing intensified atmospheric demand under anthropogenic warming (Boisier et al., 2018).

4.3. Spatial versus temporal variation in WUE-drought relationships

The two-way fixed-effects panel regression revealed an important analytical distinction: the cross-sectional associations between drought indices and WUE (mean temporal $R^2 = 0.172$-0.181 for SPI and SPEI) reflect the chronic spatial gradient in aridity across Chile more than they reflect year-to-year within-watershed dynamics. Once watershed fixed effects absorb time-invariant characteristics, aridity zone, crop system, soil type, irrigation access; the within-watershed temporal association between drought indices and WUE is non-significant for SPEI, SPI, and EDDI across all 76 watersheds. Only zNPP, which directly tracks the NPP numerator of WUE, retains significance in the within-watershed temporal dimension.

This spatial-versus-temporal distinction has direct implications for how the results should be interpreted. The primary contribution of this paper is in characterizing the *spatial* structure of WUE drought sensitivity: where the megadrought has concentrated its impacts (central Mediterranean zone), which crop systems amplify that impact (perennial horticultural), and what the spatial extent and clustering of vulnerability looks like (Moran's $I = 0.627$). The panel regression does not invalidate these spatial findings; it clarifies that the aridification signal is spatially organized rather than temporally reactive at the annual within-watershed scale.

Restricting the panel to Chilean Matorral watersheds ($n = 16$) yielded significant SPEI ($\beta = 0.124$, $\rho = 0.006$) and SPI ($\beta = 0.085$, $\rho = 0.012$) associations while EDDI remained non-significant ($\beta = 0.001$, $\rho = 0.979$), confirming geographic dilution as the source of all-watershed non-significance. A post-2010 interaction

term showed only a marginal SPEI effect ($\beta = 0.079$, $\rho = 0.056$), indicating that the megadrought WUE decline operates predominantly through the chronic spatial aridity gradient rather than an abrupt shift in within-watershed temporal sensitivity.

The sign reversal between the all-watershed SPEI coefficient ($= -0.009$, NS) and the Mediterranean-subset coefficient ($\beta = +0.124$, $\rho = 0.006$) reflects confounding by southern watersheds, where cloudier wet years suppress NPP relative to ET, the opposite of the moisture-limited Mediterranean response. The Mediterranean-subset result is the ecologically meaningful within-watershed WUE-SPEI sensitivity; the all-watershed null reflects geographic heterogeneity rather than absent drought-WUE coupling.

4.4. Crop composition as a moderator of drought sensitivity

The finding that perennial horticultural watersheds exhibit higher WUE-SPEI sensitivity than annual or forage systems is interpreted as a spatial association between crop composition and drought sensitivity, not as evidence of direct causation. Higher sensitivity means that WUE fluctuates more strongly with the hydroclimatic balance signal, it increases more in wet years and decreases more in dry years. Under prolonged drought such as the megadrought, this implies that perennial-dominated zones face disproportionately large WUE penalties. Given that Chile's export-oriented fruit and wine sectors are concentrated in precisely these Mediterranean-climate watersheds, the economic exposure to aridification is amplified by the crop composition of these zones (Fernández et al., 2023).

This spatial association is unlikely to be solely an artefact of drought-driven crop composition change. A potential concern is that the 2020-2021 census composition may partly reflect adaptive responses to the preceding megadrought, for example, abandonment of water-intensive annual crops and retention of higher-value perennials. However, the pre-drought (2007) watershed-level baseline regression (n = 75; R^2 = 0.306; Supplementary Figure S-1) was directionally consistent with the 2021 results. Cereal proportion was a significant negative predictor in both the 2007 OLS ($\beta = -0.202$, $\rho = 0.010$) and the 2021 SEM (β = -0.154, $\rho = 0.040$). Fruit tree proportion was positive in both years (2021 OLS: $\beta = 0.213$, $\rho < 0.001$; 2007 OLS: $\beta = 0.142$, $\rho = 0.075$) but did not reach significance in the spatial error models for either year. The directional consistency of the cereal effect, the most robust predictor across all model specifications, supports the interpretation that the crop composition-sensitivity relationship reflects a structural property of agricultural land use rather than a purely adaptive reorganization in response to drought. The evidence for the perennial (fruit tree) effect is weaker under spatial error correction and should be interpreted cautiously.

This association is consistent with physiology: perennials sustain large permanent canopy structures that amplify WUE fluctuations, while annuals buffer GPP loss through shorter growing cycles and earlier senescence; forage systems show lower base WUE sensitivity (Chakraborti et al., 2023; Davis et al., 2017). The NPP/ET decomposition analysis confirms that this perennial sensitivity operates primarily through the NPP numerator: vineyard proportion was a significant predictor of zNPP-SPEI sensitivity in the spatial error model ($\beta = 0.769$, p = 0.036) but the ET denominator response (SETI-SPEI SEM: $\beta = 0.582$, p = 0.137) did not survive spatial correction, suggesting that droughts suppress vine productivity more strongly than they reduce vineyard evapotranspiration, consistent with deep-rooted perennials maintaining partial water uptake under moisture stress.

These results complement the global literature on crop-water relationships (Boser et al., 2024; Wang et al., 2024) by demonstrating that the composition of agricultural land use fundamentally shapes the WUE response to aridification at the regional scale. Policies aimed at improving agricultural water use efficiency in Chile during prolonged drought should account for this crop-composition modulation effect, recognizing that perennial-dominated watersheds require more adaptive water governance than annual crop systems (FAO y ONU Agua, 2025; Hellegers and Van Halsema, 2021).

4.5. Spatial structure and governance implications

The strong spatial autocorrelation in WUE trends-confirmed by Moran's I and the Gi* hotspot analysis—indicates that the megadrought's impact on agricultural WUE is not atomistic at the watershed level but organized into large coherent spatial patterns. This spatial structure has direct implications for water governance: the most drought-affected zones form geographic clusters in which water stress is likely to compound across watersheds simultaneously, reducing the potential for spatial redistribution of water resources to buffer impacts (Budds, 2020; Rivera et al., 2016).

The spatial clustering of WUE coldspots in the central Mediterranean zone, where Chile's most economically important irrigated agriculture is concentrated, represents a critical vulnerability nexus. Under continued aridification, the convergence of high crop sensitivity (perennial systems), strong hydroclimatic stress (megadrought), and spatial clustering of WUE decline could accelerate the economic and ecological consequences of insufficient adaptive response (Fernández et al., 2023; MMA, MINAGRI, 2013).

4.6. Methodological limitations and future research

Several limitations should be acknowledged. First, WUE estimated from satellite-derived NPP/ET integrates all vegetation cover within agricultural areas and may include natural vegetation patches within watershed boundaries, introducing noise. The agricultural mask used to define WUE pixels was held static over the 2001-2020 study period. In central Chile, agricultural lands are fragmented and interspersed with native Mediterranean shrubland (matorral), which may exhibit different NPP and ET responses to drought. Because matorral distribution varies systematically along the latitudinal aridity gradient, the proportion of natural vegetation within the agricultural mask could potentially confound the observed spatial differences in WUE sensitivity. We addressed this directly by computing the natural vegetation fraction per watershed from ESA CCI-LC (2016) and including it as a control covariate in the spatial error model. Median natural vegetation fraction within agricultural pixels was 0.267 (range 0.00–0.60). The natural vegetation covariate was non-significant ($\beta = -0.017$, p = 0.810) and did not alter the primary crop composition coefficients, indicating that matorral contamination is not a material confounder of the WUE sensitivity patterns reported here.

Second, the static agricultural mask cannot distinguish active cultivation from drought-driven land abandonment. If irrigated parcels transitioned to bare soil or sparse cover during the megadrought, the resulting decline in both NPP and ET would produce WUE signals indistinguishable from active-area efficiency loss. This confound is most likely to affect rainfed cereal watersheds, where water stress can cause crop failure and partial abandonment. Future studies should cross-reference the WUE time series with annual dynamic crop extent products (e.g., GLAD Global Cropland Extent) to identify pixels that transitioned out of active agriculture during the megadrought period.

Third, the use of two cross-sectional agricultural censuses (2007 and 2020-2021) captures pre- and post-megadrought composition but cannot resolve gradual compositional change within the study period; longitudinal census data would allow analysis of how cropping system adaptation responds incrementally to drought stress. The directional consistency between 2007 and 2021 regression results reduces but does not eliminate this concern.

Fourth, central Chile's agricultural valleys depend heavily on Andean snowmelt-fed rivers for irrigation water. SPEI and SPI are calculated from local precipitation and reference evapotranspiration, and do not capture the contribution of upstream snowpack to actual irrigation water availability. In years with strong snowmelt input, irrigated crops may be buffered from meteorological drought signals that SPEI would classify as severe.

This decoupling between local meteorological drought and actual irrigation water availability is particularly relevant for perennial horticultural crops, which are predominantly irrigated by snowmelt-fed river systems, and may cause the WUE-SPEI sensitivity of these systems to be underestimated or mischaracterized. Future research should explicitly integrate hydrological drought indices such as Snow Water Equivalent (SWE) anomalies or streamflow-based indices such as the Streamflow Drought Index (Lema et al., 2025) to capture the buffering effect of upstream snowpack. This would allow separation of meteorological from hydrological drought effects on WUE in Andean-fed agricultural systems and provide a more logically coherent framework for evaluating crop-specific vulnerability in these irrigation-dependent regions.

Future research should examine WUE dynamics at sub-seasonal scales to capture phenological shifts, integrate irrigation infrastructure data (excluded from this paper per scope definition) to more precisely distinguish irrigated from rainfed WUE responses, and extend the analysis into the 2021-2025 period to assess whether the megadrought's hydroclimatic signal has intensified or abated. The census-based crop composition analysis presented here provides a methodological template that can be applied to evaluate whether agricultural adaptation—through crop switching or intensification—is modifying WUE trajectories over time (Chakraborti et al., 2023; Xie et al., 2023).

5. Conclusions

This study provides a multi-method characterization of agricultural WUE responses to the Central Chile Megadrought (2010-2020) across the country's hydrological watershed network. The principal conclusions are:

1. **WUE trends are spatially heterogeneous and predominantly negative in central Chile.** Mann-Kendall trend analysis confirmed declining WUE across the Mediterranean-climate zone (n = 76 watersheds), consistent with the megadrought's documented hydroclimatic footprint.
2. **WUE change points are temporally associated with megadrought onset.** Pettitt tests detected raw-significant change points in 17 of 76 watersheds, with 71% of those breaks occurring within ±2 years of 2010. None survived FDR correction, reflecting the limited power of individual non-parametric tests on spatially correlated 20-year series. The spatial concentration of near-2010 breaks in the central Mediterranean zone provides geographic corroboration of megadrought-associated timing, though spatial autocorrelation in break years (Moran's I = 0.164, p = 0.011) prevents formal inference about temporal clustering from independence-based tests.

3. **SPEI and SPI show comparable temporal explanatory power for WUE variability; both outperform EDDI.** Mean temporal R^2 was 0.181 (SPEI) and 0.172 (SPI), a difference not statistically significant across watersheds. EDDI was significantly weaker (mean $R^2 = 0.113$, $\rho < 0.001$ vs. both). This indicates that at the 36-month accumulation scale, the precipitation signal captures most of the WUE variance, with the atmospheric demand component adding small but detectable independent explanatory power (mean partial ρ with SPEI controlled = 0.041 vs. unconditional $\rho = 0.069$).
4. **The WUE-drought relationship is primarily spatial, not temporal, but the core megadrought zone exhibits within-watershed coupling.** Two-way fixed-effects panel regressions show non-significant within-watershed associations across all 76 watersheds, indicating that cross-sectional correlations reflect the chronic aridity gradient rather than year-to-year within-watershed dynamics. Only zNPP is significant in the temporal panel dimension. When restricted to Mediterranean-zone watersheds (Chilean Matorral, n = 16), SPEI and SPI become significant, confirming geographic dilution as the source of all-watershed non-significance. The primary analytical contribution is characterization of the *spatial* structure of WUE sensitivity, concentrated in the central Mediterranean zone where within-watershed temporal coupling is also detectable.
5. **Crop composition is spatially associated with WUE sensitivity, with cereal proportion as the most robust predictor.** Watersheds dominated by perennial horticultural crops exhibited higher WUE-SPEI sensitivity than annual or forage systems in the OLS model. A spatial error model attenuated the fruit-tree coefficient to non-significance, while cereal proportion remained a significant negative predictor ($= -0.154$, p = 0.040) and irrigated area became a significant positive predictor ($= +0.084$, p = 0.022). The cereal effect — lower WUE-SPEI sensitivity relative to forage/pasture — is the most robust finding under the spatial error specification. Cereal proportion was also a significant negative predictor in the pre-drought 2007 watershed-level regression ($= -0.202$, p = 0.010), supporting a structural rather than purely adaptive interpretation of this effect. NPP/ET component decomposition shows that vineyard sensitivity operates primarily through the NPP numerator (zNPP-SPEI SEM: $=$ 0.769, p = 0.036), while the ET denominator response does not survive spatial correction, indicating that droughts suppress vine productivity more than vineyard evapotranspiration. Natural vegetation contamination within the agricultural mask (median fraction = 0.267) was tested as a control covariate and was non-significant ($= -0.017$, p = 0.810), confirming that matorral fragmentation does not drive the crop composition–sensitivity associations.
6. **WUE responses are spatially clustered.** Moran's I and Gi* statistics confirm that WUE trends

and drought sensitivity form coherent geographic clusters, with the highest drought impact concentrated in the central Mediterranean zone.

These findings collectively demonstrate that the Central Chile Megadrought has not only reduced mean WUE but has reorganized the statistical structure of agricultural water use efficiency in ways that reflect persistent aridification rather than episodic drought. Managing agricultural water use under continued aridification will require governance frameworks that account for the multidimensional nature of drought, the spatial association between crop system composition and drought sensitivity, and the spatially clustered geography of vulnerability.

6. Acknowledgements

The authors acknowledge the use of the CASEarth global cropland WUE dataset (Jiang et al., 2025), MODIS Terra products (MOD17A3HGF, MOD16A2GF) distributed by NASA Earthdata, and ERA5-Land reanalysis data provided by the European Centre for Medium-Range Weather Forecasts (ECMWF) via the Copernicus Climate Change Service. Agricultural census microdata were obtained from the Chilean Instituto Nacional de Estadísticas (INE). [Funding sources, grant numbers, and institutional affiliations to be completed upon acceptance.] The authors declare no conflicts of interest.

7. Code and Data Availability

All analysis code is provided as Supplementary Material for reviewer access (R scripts for all preprocessing, statistical analysis, and figure generation steps, with package versions managed via `renv` for reproducibility). A permanent citable archive with a DOI will be deposited at Zenodo upon acceptance, and the full repository will be made publicly available at that time. https://github.com/frzambra/WUE_article

Annual cropland WUE rasters (NPP/ET, 1 km, 2001-2020) were obtained from Jiang et al. (2025), available at the CASEarth Data Platform (https://data.casearth.cn/dataset/640f0132819aec3f2b52a4bb). NPP data (zNPP) were obtained from MOD17A3HGF (MODIS Terra, 500 m, Collection 6.1) and ET data (SETI) from MOD16A2GF (MODIS Terra, 500 m 8-day, Collection 6.1), both available from NASA Earthdata (https://earthdata.nasa.gov). Drought index raster time series (SPEI, SPI, EDDI) were computed from ERA5-Land monthly meteorological reanalyses. Agricultural census microdata for the 2007 and 2020-2021 censuses are publicly available from the Chilean Instituto Nacional de Estadísticas (INE; https://www.ine.gob.cl). Full software version details are listed in §2.6.

References

Aceituno, P., Boisier, J.P., Garreaud, R., Rondanelli, R., Rutllant, J.A., 2021. Climate and weather in chile, in: Fernández, B., Gironás, J. (Eds.), Water Resources of Chile. Springer International Publishing. volume 8, pp. 7–29.

AghaKouchak, A., Farahmand, A., Melton, F.S., Teixeira, J., Anderson, M.C., Wardlow, B.D., Hain, C.R., 2015. Remote sensing of drought: Progress, challenges and opportunities. Reviews of Geophysics 53, 452–480. doi:10.1002/2014RG000456.

Bivand, R., Millo, G., Piras, G., 2021. A Review of Software for Spatial Econometrics in R. Mathematics 9, 1276. URL: https://www.mdpi.com/2227-7390/9/11/1276, doi:10.3390/math9111276.

Bivand, R., Wong, D.W.S., 2018. Comparing implementations of global and local indicators of spatial association. TEST 27, 716–748. doi:10.1007/s11749-018-0599-x.

Boisier, J., Alvarez-Garreton, C., Cordero, R., Damiani, A., Gallardo, L., Garreaud, R., Lambert, F., Ramallo, C., Rojas, M., Rondanelli, R., 2018. Anthropogenic drying in central-southern chile evidenced by long-term observations and climate model simulations. Elementa 6, 74. doi:10.1525/elementa.328.

Boser, A., Caylor, K., Larsen, A., Pascolini-Campbell, M., Reager, J., Carleton, T., 2024. Field-scale crop water consumption estimates reveal potential water savings in california agriculture. Nature Communications 15, 2366. doi:10.1038/s41467-024-46031-2.

Budds, J., 2020. Securing the market: Water security and the internal contradictions of chile's water code. Geoforum 113, 165–175. doi:10.1016/j.geoforum.2018.09.027.

Chakraborti, R., Davis, K.F., DeFries, R., Rao, N.D., Joseph, J., Ghosh, S., 2023. Crop switching for water sustainability in india's food bowl yields co-benefits for food security and farmers' profits. Nature Water 1, 864–878. doi:10.1038/s44221-023-00135-z.

Croissant, Y., Millo, G., 2008. Panel data econometrics in R: The plm package. Journal of Statistical Software 27, 1–43. doi:10.18637/jss.v027.i02.

Davis, K., Rulli, M., Seveso, A., D'Odorico, P., 2017. Increased food production and reduced water use through optimized crop distribution. Nature Geoscience 10, 919–924. doi:10.1038/s41561-017-0004-5.

Dinerstein, E., Olson, D., Joshi, A., Vynne, C., Burgess, N.D., Wikramanayake, E., Hahn, N., Palminteri, S., Hedao, P., Noss, R., Hansen, M., Locke, H., Ellis, E.C., Jones, B., Barber, C.V., Hayes, R., Kormos, C., Martin, V., Crist, E., Saleem, M., 2017. An ecoregion-based approach to protecting half the terrestrial realm. BioScience 67, 534–545. doi:10.1093/biosci/bix014.

Fader, M., Shi, S., Von Bloh, W., Bondeau, A., Cramer, W., 2016. Mediterranean irrigation under climate change: more efficient irrigation needed to compensate for increases in irrigation water requirements. Hydrology and Earth System Sciences 20, 953–973. URL: https://hess.copernicus.org/articles/20/953/2016/, doi:10.5194/hess-20-953-2016.

FAO y ONU Agua, 2025. Progreso del cambio en la eficiencia del uso del agua. doi:10.4060/cd2023es.

Fernández, F., Vásquez-Lavín, F., Ponce, R., Garreaud, R., Hernández, F., Link, O., Zambrano, F., Hanemann, M., 2023. The economics impacts of long-run droughts: Challenges, gaps, and way forward. Journal of Environmental Management 344, 118726. doi:10.1016/j.jenvman.2023.118726.

Folke, C., Carpenter, S., Walker, B., Scheffer, M., Elmqvist, T., Gunderson, L., Holling, C.S., 2004. Regime shifts, resilience, and biodiversity in ecosystem management. Annual Review of Ecology, Evolution, and Systematics 35, 557–581. doi:10.1146/annurev.ecolsys.35.021103.105711.

Fox, J., Weisberg, S., 2019. An R Companion to Applied Regression. 3 ed., Sage, Thousand Oaks, CA.

Garreaud, R., Alvarez-Garreton, C., Barichivich, J., Boisier, J., Christie, D., Galleguillos, M., LeQuesne, C., McPhee, J., Zambrano-Bigiarini, M., 2017. The 2010-2015 mega drought in central chile: Impacts on regional hydroclimate and vegetation. Hydrology and Earth System Sciences Discussions 2017, 1–37. doi:10.5194/hess-2017-191.

Garreaud, R., Boisier, J., Rondanelli, R., Montecinos, A., Sepúlveda, H., Veloso-Aguila, D., 2020. The central chile mega drought (2010–2018): A climate dynamics perspective. International Journal of Climatology 40, 421–439. doi:10.1002/joc.6219.

Gebrechorkos, S.H., Peng, J., Dyer, E., Miralles, D.G., Vicente-Serrano, S.M., Funk, C., Beck, H.E., Asfaw, D.T., Singer, M.B., Dadson, S.J., 2023. Global high-resolution drought indices for 1981–2022. Earth System Science Data 15, 5449–5466. doi:10.5194/essd-15-5449-2023.

Gebrechorkos, S.H., Sheffield, J., Vicente-Serrano, S.M., Funk, C., Miralles, D.G., Peng, J., Dyer, E., Talib,

J., Beck, H.E., Singer, M.B., Dadson, S.J., 2025. Warming accelerates global drought severity. Nature doi:10.1038/s41586-025-09047-2.

Hellegers, P., Van Halsema, G., 2021. Sdg indicator 6.4.1 "change in water use efficiency over time": Methodological flaws and suggestions for improvement. Science of The Total Environment 801, 149431. doi:10.1016/j.scitotenv.2021.149431.

Hijmans, R.J., 2025. terra: Spatial Data Analysis. URL: https://CRAN.R-project.org/package=terra, doi:10.32614/CRAN.package.terra. r package version 1.8-54.

Hobbins, M.T., Wood, A., McEvoy, D.J., Huntington, J.L., Morton, C., Anderson, M., Hain, C., 2016. The evaporative demand drought index. part i: Linking drought evolution to variations in evaporative demand. Journal of Hydrometeorology 17, 1745–1761. doi:10.1175/JHM-D-15-0121.1.

Hoekstra, A., Mekonnen, M., 2012. The water footprint of humanity. Proceedings of the National Academy of Sciences 109, 3232–3237. doi:10.1073/pnas.1109936109.

Hoover, D., Abendroth, L., Browning, D., Saha, A., Snyder, K., Wagle, P., Witthaus, L., Baffaut, C., Biederman, J., Bosch, D., Bracho, R., Busch, D., Clark, P., Ellsworth, P., Fay, P., Flerchinger, G., Kearney, S., Levers, L., Saliendra, N., Schmer, M., Schomberg, H., Scott, R., 2023. Indicators of water use efficiency across diverse agroecosystems and spatiotemporal scales. Science of The Total Environment 864, 160992. doi:10.1016/j.scitotenv.2022.160992.

Howden, S., Soussana, J.F., Tubiello, F., Chhetri, N., Dunlop, M., Meinke, H., 2007. Adapting agriculture to climate change. Proceedings of the National Academy of Sciences 104, 19691–19696. doi:10.1073/pnas.0701890104.

Hu, G., Jia, L., 2015. Monitoring of Evapotranspiration in a Semi-Arid Inland River Basin by Combining Microwave and Optical Remote Sensing Observations. Remote Sensing 7, 3056–3087. URL: https://www.mdpi.com/2072-4292/7/3/3056, doi:10.3390/rs70303056.

INE, 2007. VII Censo nacional agropecuario y forestal. Instituto Nacional de Estadística. Informe Agropecuarias 2007. Technical Report.

INE, 2021. VIII Censo Nacional Agropecuario y Forestal. Instituto Nacional de Estadísticas. Santiago, Chile. URL: https://www.ine.gob.cl/estadisticas-por-tema/agricultura-y-medio-ambiente/censo-agropecuario. resultados finales publicados en octubre de 2022.

Ito, A., Inatomi, M., 2012. Water-use efficiency of the terrestrial biosphere: A model analysis focusing on interactions between the global carbon and water cycles. Journal of Hydrometeorology 13, 681–694. doi:10.1175/JHM-D-10-05034.1.

Jiang, M., Zheng, C., Jia, L., Chen, J., 2025. A 20-year dataset (2001–2020) of global cropland water-use efficiency at 1-km grid resolution. Scientific Data 12, 574. doi:10.1038/s41597-025-04904-1.

Kates, R., Travis, W., Wilbanks, T., 2012. Transformational adaptation when incremental adaptations to climate change are insufficient. Proceedings of the National Academy of Sciences 109, 7156–7161. doi:10.1073/pnas.1115521109.

Lema, F., Mendoza, P.A., Vásquez, N.A., Mizukami, N., Zambrano-Bigiarini, M., Vargas, X., 2025. Technical note: What does the Standardized Streamflow Index actually reflect? Insights and implications for hydrological drought analysis. Hydrology and Earth System Sciences 29, 1981–2002. URL: https://hess.copernicus.org/articles/29/1981/2025/, doi:10.5194/hess-29-1981-2025.

Li, F., Xiao, J., Chen, J., Ballantyne, A., Jin, K., Li, B., Abraha, M., John, R., 2023. Global water use efficiency saturation due to increased vapor pressure deficit. Science 381, 672–677. doi:10.1126/science.adf5041.

McEvoy, D.J., Huntington, J.L., Hobbins, M.T., Wood, A., Morton, C., Anderson, M., Hain, C., 2016. The evaporative demand drought index. part ii: Conus-wide assessment against common drought indicators. Journal of Hydrometeorology 17, 1763–1779. doi:10.1175/JHM-D-15-0122.1.

Mckee, T.B., Doesken, N.J., Kleist, J., 1993. The relationship of drought frequency and duration to time scales, in: Proceedings of the Ninth Conference on Applied Climatology, American Metereological Society, Boston. pp. 179–184.

Mekonnen, M.M., Hoekstra, A.Y., 2011. The green, blue and grey water footprint of crops and derived crop products. Hydrology and Earth System Sciences 15, 1577–1600. URL: https://hess.copernicus.org/articles/15/1577/2011/, doi:10.5194/hess-15-1577-2011.

MMA, MINAGRI, 2013. Plan de Adaptación al Cambio Climático del Sector Silvoagropecuario: Propuesta Ministerial elaborada en el marco del Plan de Acción Nacional de Cambio Climático 2008-2012. Ministerio de Medio Ambiente / Ministerio de Agricultura, Gobierno de Chile, Santiago, Chile.

Patakamuri, S.K., O'Brien, N., 2021. modifiedmk: Modified Versions of Mann Kendall and Spearman's Rho

Trend Tests. URL: https://CRAN.R-project.org/package=modifiedmk, doi:10.32614/CRAN.package.modifiedmk. r package version 1.6.

Pebesma, E., 2018. Simple Features for R: Standardized Support for Spatial Vector Data. The R Journal 10, 439–446. URL: https://doi.org/10.32614/RJ-2018-009, doi:10.32614/RJ-2018-009.

Pebesma, E., Bivand, R., 2023. Spatial Data Science: With applications in R. Chapman and Hall/CRC. URL: https://r-spatial.org/book/, doi:10.1201/9780429459016.

Pedersen, T.L., 2025. patchwork: The Composer of Plots. URL: https://CRAN.R-project.org/package=patchwork, doi:10.32614/CRAN.package.patchwork. r package version 1.3.1.

Pettitt, A.N., 1979. A non-parametric approach to the change-point problem. Journal of the Royal Statistical Society: Series C (Applied Statistics) 28, 126–135. doi:10.2307/2346729.

Pohlert, T., 2023. trend: Non-Parametric Trend Tests and Change-Point Detection. URL: https://CRAN.R-project.org/package=trend, doi:10.32614/CRAN.package.trend. r package version 1.1.6.

R Core Team, 2025. R: A Language and Environment for Statistical Computing. R Foundation for Statistical Computing. Vienna, Austria. URL: https://www.R-project.org/.

Rivera, D., Godoy-Faúndez, A., Lillo, M., Alvez, A., Delgado, V., Gonzalo-Martín, C., Menasalvas, E., Costumero, R., García-Pedrero, Á., 2016. Legal disputes as a proxy for regional conflicts over water rights in chile. Journal of Hydrology 535, 36–45. doi:10.1016/j.jhydrol.2016.01.057.

Running, S., Mu, Q., Zhao, M., Moreno, A., 2021. MODIS/Terra net evapotranspiration Gap-Filled 8-day L4 global 500m SIN grid V061.

Tennekes, M., 2018. tmap: Thematic maps in R. Journal of Statistical Software 84, 1–39. doi:10.18637/jss.v084.i06.

Vicente-Serrano, S.M., Beguería, S., López-Moreno, J.I., 2010. A multiscalar drought index sensitive to global warming: The standardized precipitation evapotranspiration index. Journal of Climate 23, 1696–1718. doi:10.1175/2009JCLI2909.1.

Wallace, J., 2000. Increasing agricultural water use efficiency to meet future food production. Agriculture, Ecosystems & Environment 82, 105–119. URL: http://dx.doi.org/10.1016/S0167-8809(00)00220-6, doi:10.1016/s0167-8809(00)00220-6.

Wang, T., Sun, S., Yin, Y., Zhao, J., Tang, Y., Wang, Y., Gao, F., Luan, X., 2024. Status of crop water use efficiency evaluation methods: A review. Agricultural and Forest Meteorology 349, 109961. doi:10.1016/j.agrformet.2024.109961.

Wickham, H., 2016. ggplot2: Elegant Graphics for Data Analysis. Springer-Verlag New York. URL: https://ggplot2.tidyverse.org.

Wickham, H., Averick, M., Bryan, J., Chang, W., McGowan, L.D., François, R., Grolemund, G., Hayes, A., Henry, L., Hester, J., Kuhn, M., Pedersen, T.L., Miller, E., Bache, S.M., Müller, K., Ooms, J., Robinson, D., Seidel, D.P., Spinu, V., Takahashi, K., Vaughan, D., Wilke, C., Woo, K., Yutani, H., 2019. Welcome to the tidyverse. Journal of Open Source Software 4, 1686. doi:10.21105/joss.01686.

Xie, W., Zhu, A., Ali, T., Zhang, Z., Chen, X., Wu, F., Huang, J., Davis, K., 2023. Crop switching can enhance environmental sustainability and farmer incomes in china. Nature 616, 300–305. doi:10.1038/s41586-023-05799-x.

Yu, L., Gao, X., Zhao, X., 2020. Global synthesis of the impact of droughts on crops' water-use efficiency (WUE): Towards both high WUE and productivity. Agricultural Systems 177, 102723. URL: https://linkinghub.elsevier.com/retrieve/pii/S0308521X19301568, doi:10.1016/j.agsy.2019.102723.

Zambrano, F., Vrieling, A., Meza, F., Duran-Llacer, I., Fernández, F., Venegas-González, A., Raab, N., Craven, D., 2025. From Drought to Aridification: Land-Cover Fingerprints of a Drying Chile. Earth's Future 13, e2025EF006744. URL: https://agupubs.onlinelibrary.wiley.com/doi/10.1029/2025EF006744, doi:10.1029/2025EF006744.

Supplementary Material

Supplementary Table S-1 — Sample sizes by analytical step

Analysis	n	Spatial unit	Notes
WUE trend (Mann-Kendall)	76	Watershed	Agricultural watersheds with complete 2001-2020 WUE data

Analysis	n	Spatial unit	Notes
WUE-SPEI sensitivity (OLS slope)	76	Watershed	Same set; one per-watershed regression per index
Panel regression (two-way FE)	76	Watershed	Balanced panel; 76 × 20 = 1,520 watershed-year obs. minus missing
Panel regression — Mediterranean subset	16	Watershed	Chilean Matorral ecoregion watersheds; panel N = 16 × 20 = 320 watershed-year obs.
Crop composition OLS (2021 census)	75	Watershed	76 minus 1 watershed with missing irrigation data
Crop composition spatial error model (2021)	75	Watershed	Same set; `spatialreg::errorsarlm`, queen contiguity
Crop composition OLS (2007 baseline)	75	Watershed	2007 VII Census proportions aggregated to watershed level via `comcuen.rds` spatial join; $R^2 = 0.306$
Crop composition SEM (2007 baseline)	75	Watershed	`spatialreg::errorsarlm`, queen contiguity; $\lambda = 0.731$, $p < 0.001$

Supplementary Table S-2 — Ecoregion-stratified Wilcoxon signed-rank tests

Wilcoxon signed-rank tests comparing mean WUE in the pre-megadrought (2001-2009) versus megadrought (2010-2020) periods, stratified by ecoregion. Hodges-Lehmann median difference and 95% confidence interval are reported alongside p-values. Full numerical results are available in

outputs/tables/wilcox_by_ecoregion.csv.

Supplementary Figure S-1 — Pre-drought (2007) crop composition and WUE sensitivity

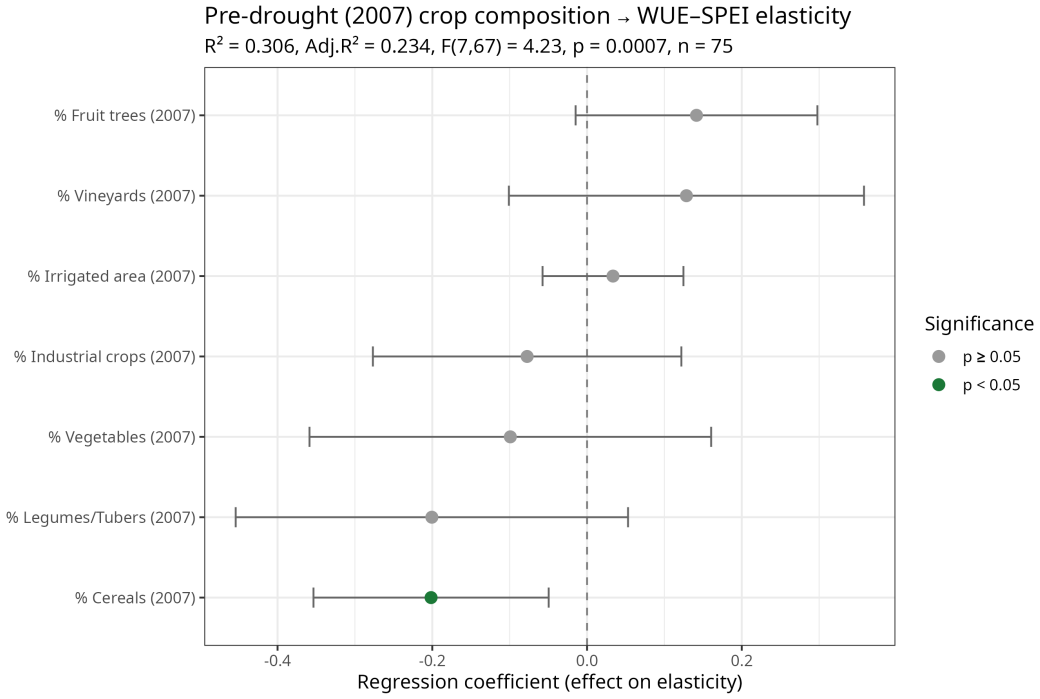

Figure 10: Pre-drought (2007) crop composition as a predictor of WUE-SPEI sensitivity. OLS and spatial error model (SEM) regression coefficient plots using VII Agricultural and Forestry Census (2007) proportions aggregated to watershed level as predictors (reference category: forage/pasture; n = 75 watersheds). The cereal coefficient is directionally consistent with the 2021 SEM result, supporting a structural rather than purely adaptive interpretation. OLS: $R^2 = 0.306$, $F(7,67) = 4.23$, $p < 0.001$. SEM: $= 0.731$, $p < 0.001$.